Article

Rauwolfia serpentina Treatment Prevents Oxidative Stress, Inflammation, and Fibrosis in the Heart and Kidneys of Isoprenaline-Administered Rats

Kamrun Nahar Ela [1], Mirza Alimullah [1], Asif Ul Haque Shuvo [1], Puspa Sornakar [1], Shamima Sultana [1], Md. Junaeid Rahman [1], Md. Sakil Amin [2], Khondoker Shahin Ahmed [3], Hemayet Hossain [3], Mohammad Borhan Uddin [1], Ferdous Khan [1], Md. Ashraful Alam [1,*], and Nusrat Subhan [1,*]

[1] Department of Pharmaceutical Sciences, North South University, Dhaka 1229, Bangladesh
[2] Department of Pharmacy, University of Developmental Alternative, Dhaka 1209, Bangladesh
[3] BCSIR Laboratories, Bangladesh Council of Scientific and Industrial Research (BCSIR), Dhaka 1205, Bangladesh
* Correspondence: ashraful.alam@northsouth.edu (M.A.A.); nusrat.subhan@northsouth.edu (N.S.)
Received: 30 December 2025; Revised: 11 February 2026; Accepted: 25 February 2026; Published: 24 March 2026

Abstract: This study examined the protective effects of *Rauwolfia serpentina* root extract against isoprenaline (ISO)-induced oxidative stress, fibrosis, and cardiac injury in rats. ISO (50 mg/kg) was administered subcutaneously twice weekly. Biochemical markers, including uric acid, creatinine, CK-MB, MDA, NO, AOPP, and antioxidant enzymes, were evaluated, alongside histopathological analysis. ISO increased oxidative stress, inflammation, and cardiac damage, while *R. serpentina* treatment significantly reduced uric acid, creatinine, CK-MB, MDA, NO, AOPP, and myeloperoxidase levels, and restored antioxidant activity. Histology showed reduced fibrosis and inflammatory infiltration in treated rats. Gene expression analysis revealed downregulation of NF-κB, TNF-α, and IL-6, along with activation of the Nrf2-HO-1 pathway. Network pharmacology identified six key polyphenols in *R. serpentina* interacting with 141 cardiac hypertrophy-related proteins. Overall, *R. serpentina* mitigates ISO-induced cardiac and renal damage by reducing oxidative stress, inflammation, and fibrosis.

Keywords: *Rauwolfia serpentina*; myocardial damage; isoprenaline; fibrosis; inflammation

1. Introduction

The coexistence of cardiac and renal disease significantly elevates both mortality and morbidity [1]. In the last several decades, the medical community has placed greater emphasis on the strong link between cardiovascular disease and chronic kidney disease (CKD). The fact that heart and renal problems frequently coincide and affect one another is becoming increasingly apparent. This complex relationship can even result in the simultaneous failure of both organs, a condition referred to as cardiorenal syndrome [2]. Among CKD patients, heart failure is the primary cardiovascular complication, and its prevalence rises as kidney function declines [3].

The development of myocardial infarction (MI) involves a series of intricate processes, commencing with pre-occlusion mechanisms linked to atherosclerosis. This chronic inflammatory condition represents the critical initial phase in the development of myocardial infarction (MI) and progresses to post-occlusion events involving plaque rupture and subsequent ischemia/reperfusion injury [4]. High blood sugar, cholesterol, and blood pressure contribute to its initiation and progression [5]. The following risk factors might culminate in oxidative stress on the endothelium, triggering abnormalities in the functioning of the endothelium. This impaired function allows low-density lipoprotein to breach the inner lining of the artery wall and inflict damage, leading to the initiation of plaque instigation and straitening of the arteries [6]. Following the obstruction of blood flow, myocardial ischemia arises from the formation of blood clots after the rupture of arterial plaques. The interaction between mitochondrial ROS and polyunsaturated fats, particularly cardiolipin, produces detrimental byproducts comprised of malondialdehyde and 4-hydroxy-2-nominal [7]. Cells have built-in antioxidant defense mechanisms to offset the damaging effects of ROS [8]. Necessary antioxidant enzymes involved in ROS regulation include superoxide dismutase, glutathione S-transferase, and catalase. Nuclear factor erythroid 2-related factor 2 (NRF2), the vital

Copyright: © 2026 by the authors. This is an open access article under the terms and conditions of the Creative Commons Attribution (CC BY) license (https://creativecommons.org/licenses/by/4.0/).
Publisher's Note: Scilight stays neutral with regard to jurisdictional claims in published maps and institutional affiliations.

regulator in response to oxidative stress during myocardial infarction, influences the transcriptional levels of antioxidant genes by binding to their promoters [9].

One chronic condition that may give rise to Acute Kidney Injury (AKI) is acute myocardial infarction (AMI) [10]. Numerous individuals having chronic kidney disease (CKD) are more inclined to have risk factors associated with the pathophysiology of CKD, as well as traditional cardiovascular risk markers, which increase their susceptibility to AMI [10]. The underlying mechanisms of heart failure (HF) as well as chronic kidney disease (CKD) heavily rely on the RAAS, also known as the renin-angiotensin-aldosterone system (RAAS) and sympathetic nervous system (SNS). In HF, the activation of RAAS and SNS is crucial for regulating blood pressure and maintaining extracellular fluid volume [11]. However, prolonged activation of these systems can have adverse effects, including the progression of CKD. Studies have demonstrated that increased SNS and RAAS activity, particularly through angiotensin II (Ang II), contributes to kidney damage by generating reactive oxygen species (ROS) and causing podocyte injury, leading to albuminuria [12]. RAAS is also a significant contributor to fibrosis, a common consequence of heart and kidney damage, primarily triggered through the transforming growth factor-beta (TGF-β) pathway [13]. Aldosterone, a key hormone within RAAS, escalates renal and cardiac fibrosis and inflammatory conditions by activating myofibroblasts and promoting extracellular matrix (ECM) accumulation. Isoprenaline, a synthetic catecholamine, has been utilized as a model to investigate cardiomyopathy because of its capacity to induce necrosis in heart cells and myocardial infarction [14]. It produces highly cytotoxic free radicals and induces lipid peroxidation, causing the membranes of the heart to sustain severe damage [15]. Cardiotoxicity induced by isoprenaline is partially attributed to an overload of intracellular calcium, resulting in alterations in ion permeability across the cell membrane, which leads to an excess of calcium and can harm cells by activating calcium-dependent enzymes and disrupting mitochondrial energy production. This disturbance in energy production could contribute to the development of cardiomyopathy [16].

Rauwolfia serpentina (L.) Benth. ex Kurz, part of the Apocynaceae family, is a perennial plant indigenous to Bangladesh, India, and several other regions of Asia and is well known for its profound effects on public health [17,18]. An integral part of conventional healthcare, it is particularly known in Ayurveda as Sarpagandha [19]. *R. serpentina* is a well-known plant with exceptional medicinal properties, especially in producing essential drugs with anti-arrhythmic effects. The alkaloids ajmaline and reserpine, derived from this plant, have historically been used to treat circulatory diseases and hypertension [20]. Rutin, a quercetin glycoside, has numerous therapeutic applications because of its anti-inflammatory, neuroprotective, cardiovascular, antioxidant, and anticancer effects [21]. It contains flavonoids known for their antioxidant properties. Research conducted on cells in a controlled environment and on animals indicates that flavonoids, with their antioxidant and antimutagenic properties, could help mitigate the risk of stroke and cardiovascular disease [22,23]. Additionally, *R. serpentina* contains tannins that help limit oxidation, as it contains gallic acid [24]. *R. serpentina* has demonstrated impressive antioxidant properties, according to tests using 2,2-diphenyl-1-picryl hydrazyl radical scavenging (DPPH) and ferric reducing antioxidant power (FRAP), flavonoids are the active ingredient that causes this effect [25]. In vitro studies have indicated that the alkaloids in *R. serpentina*, likely reserpine [26] and yohimbine [27], exhibit effective anticancer properties. Researchers investigated the methanol extract of *R. serpentina* for its potential to scavenge free radicals in an albino rat model of CCl4-induced liver injury [26]. A study involving albino rats revealed that an aqueous methanolic extract of *R. serpentina* exhibited significant antihypertensive and antihyperlipidemic effects [27]. The methanolic root extract of *R. serpentina* has the potential to increase insulin levels, lower elevated blood sugar, and reduce triglyceride and cholesterol levels in mice with fructose-induced Type 2 diabetes [28]. Recent research suggests that alkaloid-rich plants have potent antibacterial properties due to their high content of saponins, tannins, and flavonoids [29]. There is a scarcity of comprehensive studies on the therapeutic evaluation and phytochemical testing of *R. serpentina*, although a few prior studies have provided data suggesting its therapeutic potential [26–28]. In this current study, the cardio-renal protective benefits of *R. serpentina* root extract were evaluated in ISO-administered rats.

2. Materials & Methods

2.1. Chemicals and Reagents

Methanol (HPLC), ethanol, acetic acid (HPLC), and acetonitrile (HPLC) were procured from Merck (Darmstadt, Germany). Syringic acid, (+)-catechin hydrate, ellagic acid, vanillic acid, vanillin, (−)-epicatechin, gallic acid, *p*-coumaric acid, caffeic acid, kaempferol, rutin hydrate, rosmarinic acid, myricetin, pyrogallol, quercetin hydrate, and trans-ferulic acid were acquired from Sigma–Aldrich (St. Louis, MO, USA). Uric acid, creatinine, and CK-MB assay kits were obtained from LABKIT, Barcelona, Spain. We purchased the DreamTaq PCR Master Mix, RevertAid First Strand cDNA Synthesis Kit, Trizol RNA isolation reagent, and PowerUp SYBR

Green Master Mix Kit from Thermo-Fisher Scientific in the United States. The origin of the PCR amplification primers was Macrogen Inc. in Korea. Additional chemicals needed to measure the activities of antioxidant enzymes and indicators of oxidative stress were obtained from North South University's Departmental Chemical Store in Bangladesh.

2.2. Collection of Plant Material and Preparation of Plant Extraction

The *R. serpentina* (L.) Benth. ex Kurz plant was acquired from Purbachal area near Dhaka, in Bangladesh known for its natural resources. After obtaining a voucher specimen, the Mirpur National Herbarium identified the plant (Accession Number oacf DACB-87263). After air-drying and powdering, the root powder (50 g) was extracted with ethanol (300 mL) using a Soxhlet extractor. After filtration, the ethanol-soluble substance was collected and transferred into a 1000-milliliter round-bottom flask. It was then placed in a rotary evaporator and evaporated at 60 °C with a rotational speed of 100–120 rpm under 5 bar pressure. A rotary evaporator evaporated the ethanolic extract at lower pressure, yielding a reddish crude extract for further investigation and therapeutic rat treatment.

2.3. Analysis Using HPLC and Quantification of Polyphenolic Compounds

The HPLC-DAD analysis was used for the detection and quantification of specific phenolic compounds in the ethanolic root extract of *R. serpentina*, following the methodology described earlier [30,31]. The study used a Dionex UltiMate 3000 system with a quaternary rapid separation pump (LPG-3400RS) and a photodiode array detector (DAD-3000RS). A 4.6 × 250 mm Acclaim® C18 (5 µm) Dionex column was employed at a temperature of 30 °C, with a flow rate of 1 mL/min and an injection volume of 20 µL. The mobile phase consisted of acetonitrile (solvent A), acetic acid solution with a pH of 3.0 (solvent B), and methanol (solvent C), following a gradient elution program: 5% A/95% B (0–10 min), 10% A/90% B (11–15 min), 15% A/70% B/15% C (16–25 min), 20% A/60% B/20% C (26–30 min), 30% A/ 40% B/30% C (31–35 min), 40% A/50% B/10% C (36–40 min), and 5% A/95% B (41–45 min). A standard stock solution containing specific concentrations of various phenolic compounds was prepared in methanol for the calibration curve. In contrast, the *R. serpentina* root extract solution was prepared at 20 mg/mL in ethanol. Calibrations, peak integration, and data acquisition were done using Dionex Chromeleon software (Version 6.80 RS 10). The UV detector was set at 270 nm and applied for validation of method and analysis.

2.4. Experimental Animals

The Animal Care Unit of North South University supplied the researchers with male Long-Evans rats, aged 8 to 10 weeks and weighing 180–200 g. These rats were individually housed in wire-bottom cages and kept at 25.3 °C, with humidity ranging from 50 to 60%. They were given a regular meal and unrestrained access to water and were subjected to the 12-h light-dark cycle. The National Academy of Sciences' "Guide for Care and Use of Laboratory Animals" was strictly adhered to when conducting animal research, and the Animal Ethics Committee's approval was obtained before the investigations began. The animals were kept in customary housing [32]. The institutional IACUC committee also approved the research protocol (IACUC ID-2024/OR-NSU/IACUC/1201). This study also adhered to the ARRIVE guideline.

2.5. Treatment Protocols

The rats had to be divided into four groups in a lab environment. The first group, the control group, received drinking water and standard lab chow. Rats in Group II (ISO) received subcutaneous injections of ISO at 50 mg/kg twice weekly for 14 days. Group III (Control + *R. serpentina*) received their regular diet and water supplemented with 100 mg/kg/day of *R. serpentina* root extracts in addition to their treatment. In Group IV (ISO + *R. serpentina*), rats received 50 mg/kg of subcutaneously administered isoprenaline twice weekly and 100 mg/kg of *R. serpentina* root extracts daily for 14 days.

2.6. Animal Sacrifice and Sample Tissue Collection

All of the rats were sacrificed after 14 days with a high dose of ketamine hydrochloride at an 85 mg/kg dosage. Immediately after euthanasia, the abdomen of the rat was opened, and blood was withdrawn with the help of a syringe and needle (18 gauge) containing citrate buffer (pH 5) as an anticoagulant. The heart and kidney tissues were also surgically removed and weighed. Part of the heart and kidneys were stored in cryo-vials in a

freezer (−20 °C) for additional biochemical analyses. One part of the tissues was also preserved for mRNA isolation and gene expression study. Other parts of the tissues were preserved in neutral buffered formalin (pH 7).

2.7. Biochemical Parameters Assessment

Following blood collection, for 15 min, the samples were centrifuged at 4 °C at 4000 rpm, and the resultant plasma was separated, moved to 1.5 mL Eppendorf tubes, and kept at −20 °C until analysis [31,33]. The biochemical parameters creatinine, uric acid, and CK-MB were evaluated using the manufacturer's method (LABKIT, Barcelona, Spain). Absorbance measurements were taken at 340 nm.

2.8. Evaluation of Indicators for Oxidative Stress and Levels of Activity of Antioxidant Enzymes

At 4 °C, we spun the heart tissue at 8000 rpm for 15 min after homogenizing it in pH 7.4 phosphate buffer to measure antioxidant enzyme activity and oxidative stress markers [31]. The supernatants were then collected for enzymatic analysis and examination of oxidative stress indicators.

2.8.1. Determination of Lipid Peroxidation (LPO) as Malondialdehyde (MDA)

By detecting thiobarbituric acid reactive substances (TBARS), lipid peroxidation in cardiac and renal tissue was evaluated. The TBATCA-HCl reagent, which was made by combining identical amounts of trichloroacetic acid (15% *v*/*v*), HCl (0.25 N), thiobarbituric acid (0.37% *v*/*v*, was applied to a sample of 0.1 mL tissue homogenate (in Tris-HCl buffer at pH 7.5). After that, the combination was left to cool for 15 min in a hot water bath. A reference blank was used to test the clear supernatant's absorbance at 535 nm [34,35].

2.8.2. Determination of Nitric Oxide (NO)

We used the Griess-Illosvoy reagent to quantify nitric oxide (NO), but we modified it by substituting naphthyl ethylene diamine dihydrochloride (0.1% *w*/*v*) for 1-methylamine (5%). Heart homogenate (2 mL) was incubated for 2.5 h before being mixed with 0.5 mL of phosphate buffer saline at 25 °C. A Microplate Reader (Thermo Fisher Scientific, Waltham, MA, USA) was used to measure the absorbance of the resultant supernatant at 540 nm relative to the matching blank solution. The NO level was determined using a standard curve and expressed as nmol/g of tissue [31,36,37].

2.8.3. Determination of Advanced Oxidation Protein Products (AOPP)

Two mL of sample supernatant were diluted 1:5 with PBS to test the AOPP. Afterward, each tube received 0.1 mL of 1.16 M potassium iodide mixed with 0.2 mL of acetic acid two minutes later. Immediately after, the absorbance of the resultant mixture was measured at 340 nm compared to a blank that included 0.2 mL of acetic acid, 2 mL of PBS, and 0.1 mL of KI. Employing a chloramine-T standard curve that demonstrated a linear relationship with concentration and absorbance at 340 nm, the concentration of AOPP was derived as nmol·mL^{-1} chloramine-T equivalents inside the range of 0 to 100 nmol/mL [31,38,39].

2.8.4. Determination of Superoxide Dismutase (SOD) Activity

Using a previously published procedure, the SOD activity test was conducted on plasma, heart, and kidney tissues [31,40,41]. PBS and 2.94 mL of enzyme preparation made up the 3 mL reaction mixture. 0.06 mL epinephrine (15 mM) was added to initiate the reaction, and absorbance changes were recorded for 1 min at 480 nm at 15-s intervals. At the same time, a control without tissue homogenates was set up. One unit of enzyme activity was defined as the amount that resulted in a 50% suppression of the auto-oxidation of adrenaline in the sample solution.

2.8.5. Determination of Catalase (CAT) Activity

0.1 mL of tissue homogenate, 0.4 mL of 5.9 mM H_2O_2, and 2.5 mL of 50 mM phosphate buffer (pH 5.0) were combined to assess catalase activity. A UV–visible spectrophotometer was then used to measure the reaction mixture's absorbance at 240 nm, and any change in absorbance over the next minute was recorded. One catalase activity unit was considered an absorbance shift of 0.01 units per minute [31,42].

2.8.6. Determination of Myeloperoxidase (MPO) Activity

A technique for tracking MPO activity was developed and modified for 96-well plates using dianisidine and hydrogen peroxide. The amount of MPO produced per milligram of protein used was derived by measuring variations in absorbance at 460 nm [43,44].

2.8.7. Determination of Reduced Glutathione (GSH) Level

A 1-milliliter homogenate sample with a 10% concentration was combined with 1 mL of 4% sulfosalicylic acid to measure the amount of reduced glutathione. The samples were centrifuged at 8000 rpm for 15 min after being in an atmosphere at 4 degrees Celsius for an hour. 100 mM of 5,5-dithiobis-2-nitrobenzoic acid, 0.2 mL DTNB, 2.7 mL phosphate buffer, and 0.1 mL filtered aliquot at a pH of 7.4 made up the 3.0 mL assay mixture. A spectrophotometer was utilized to test this mixture at 412 nm immediately, and the results were reported as ng/mg protein [44,45].

2.9. Evaluation of Relative Oxidative Stress and Inflammation Regulatory Genes Level by Quantitative Real-Time Polymerase Chain Reaction (qRT-PCR)

Thermo Fisher Scientific's GeneJet RNA Purification Kit (Waltham, MA, USA) was used to separate and purify the total mRNA obtained from surgically removed heart tissue. The total mRNA amount was determined using the NanoDrop 2000 spectrophotometer (Bio-Rad, Hercules, CA, USA). Each sample was converted into cDNA using one microgramme of mRNA and the RevertAid First Strand cDNA Synthesis Kit (Thermo-Fisher Scientific, USA). Quantitative real-time PCR (qRT-PCR) utilizing Maxima SYBR Green qPCR master mixes was then used to quantify mRNA from transcription factors and enzymes linked to inflammation and oxidative stress. For qRT-PCR, forward and reverse primers were utilized, as outlined in Table 1, designed with Primer 3 online software. The following settings were used in the reaction: 1 min at 95 °C for preliminary denaturation, 40 cycles of amplification comprised of 5 s at 95 °C for denaturation, 30 s at 60 °C for annealing, 1 min at 72 °C for extension, and a final extension lasting 5 min at the same temperature. As a housekeeping gene, β-actin was utilized to normalize the transcript level of each target gene.

Table 1. This experiment will use both the forward and reverse primer sequences.

Name of Gene	Type	Sequence
Nrf-2	Forward	5′-CCC AGCACA TCC AGACAGAC-3′
	Reverse	5′-TATCCAGGGCAAGCGACT C-3′
Heme oxygenase-1 (HO-1)	Forward	5′-TGCTCGCATGAACACTCTG-3′
	Reverse	5′-TCCTCTGTCAGCAGTGCCT-3′
Heme oxygenase-2 (HO-2)	Forward	5′-CACCACTGCACTTTACTTCA-3′
	Reverse	5′-AGTGCTGGGGAGTTTTAGTG-3′
SOD	Forward	5′-GCTCTAATCACGACCCACT-3′
	Reverse	5′-CATTCTCCCAGTTGATTACATTC-3
Catalase	Forward	5′-ATTGCCGTCCGATTCTCC-3′
	Reverse	5′-CCAGTTACCATCTTCAGTGTAG-3′
Glutathione peroxidase (GPx)	Forward	5′-GGGCAAAGAAGATTCCAGGTT-3′
	Reverse	5′-GGACGGCTTCATCTTCAGTGA-3′
IL-1	Forward	5′-ATGCCTCGTGCTGTCTGACC-3′
	Reverse	5′-CCATCTTTAGGAAGACACGGGTT-3′
IL-6	Forward	5′-AGCGATGATGCACTGTCAGA-3′
	Reverse	5′-GGTTTGCCGAGTAGACCTCA-3′
TNF-α	Forward	5′-ATGTGGAACTGGCAGAGGAG-3′
	Reverse	5′-CCACGAGCAGGAATGAGAAGAG-3′
TGF-β	Forward	5′-AAGAAGTCACCCGCGTGCTA-3′
	Reverse	5′-TGTGTGATGTCTTTGGTTTTGTC-3′
iNOS	Forward	5′-TGGTCCAACCTGCAGGTCTTC-3′
	Reverse	5′-CAGTAATGGCCGACCTGATGTTG-3′
NF-κB	Forward	5′-TGTGAAGAAGCGAGACCTGGAG-3′
	Reverse	5′-GGCACGGTTATCAAAAATCGGATG-3′

2.10. Investigation into the Histopathology of Tissues

Using photomicrography, the internal structure of heart tissue, along with the degree of inflammatory cell infiltration, was observed. Before being embedded in paraffin, all tissues were fixed in neutral-buffered formalin. To detect inflammatory cells in the heart, these implanted tissues were cut into 5 μm sections using a microtome. After that, hematoxylin and eosin were used to stain them. Furthermore, fibrosis was evaluated using Sirius red staining. 40× magnification was used to capture the photomicrograph of H and E-stained sections with an Axioscope, Zeiss light microscope (Carl Zeiss, Germany). The fluorescence microscopy pictures for Sirius red-stained sections were taken in ×20 magnification with the help of Leica DM 1000 coupled with a camera Model: FLEXACAM C3 (Leica Microsystems, Wetzlar, Germany**)**.

2.11. Statistical Investigation

The mean ± standard error of the mean (SEM) was utilized to present all the test results. The One Way ANOVA and Tukey tests were employed for statistical analysis using the GraphPad Prism Software, Version 8.0.1 (GraphPad Software Inc., San Diego, CA, USA). All cases were deemed statistically significant if the *p*-value was less than 0.05 ($p < 0.05$). Principal component analysis was performed using PAST software.

2.12. Network Pharmacology and Gene Ontology analysis

2.12.1. Target Prediction for *Rauwolfia serpentina* Polyphenols

SMILES of the six major polyphenols were collected from Pubchem (https://pubchem.ncbi.nlm.nih.gov/, accessed on 29 May 2025) [46,47] and submitted to BATMAN-TCM (http://bionet.ncpsb.org.cn/batman-tcm/, accessed on 29 May 2025) [48,49], SuperPred by Charité (https://prediction.charite.de/, accessed on 29 May 2025) [50,51], TargetNet (http://targetnet.scbdd.com/, accessed on 29 May 2025) [52,53], Way2Drug (https://www.way2drug.com/, accessed on 29 May 2025) [54,55], and the Similarity Ensemble Approach (SEA); (http://sea.bkslab.org/, accessed on 29 May 2025) [56,57] for the target prediction. Outputs from all platforms were merged, and duplicates were removed, resulting in a unified, unique compilation of predicted targets among the six compounds.

2.12.2. Assembly of Cardiac Hypertrophy Gene Set

Genes associated with cardiac hypertrophy were retrieved from OMIM (https://omim.org/, accessed on 29 May 2025) [58–60] and GeneCards (https://www.genecards.org/, accessed on 29 May 2025) [61,62] using search terms and filters consistent with prior work. Entries were downloaded in gene-symbol format where available, to ensure compatibility.

2.12.3. Standardization of Identifiers

To ensure consistency in terminology, eliminate duplicates, and filter out entries without a known human ortholog, we cross-referenced and mapped all predicted targets and disease-associated genes to UniProt (https://www.uniprot.org/, accessed on 29 May 2025) [63,64].

2.12.4. Overlap Analysis

The standardized lists for polyphenol targets and cardiac hypertrophy genes were compared via an online Venn tool—Venny 2.1 (https://bioinfogp.cnb.csic.es/tools/venny/, accessed on 4 June 2025) [65,66] to extract intersecting proteins. This intersection provided a focused set of candidates for downstream network and enrichment analyses.

2.12.5. Network Pharmacology Merged and Visualization

After obtaining the intersected targets from Venny, all data were imported into Cytoscape 3.10.3(accessed on 4 June 2025) [67,68]. Networks were merged, and multiple target sets were combined. This step provided a visual merged framework linking to the effects of the polyphenols in the context of cardiac hypertrophy.

2.12.6. Protein–Protein Interaction Network

Intersecting unique targets were submitted to STRING (https://string-db.org/, accessed on 4 June 2025) [69,70] with organism set to Homo sapiens and minimum required interaction score of 0.4 (medium confidence). Interaction

data were then imported into Cytoscape version 3.10.3 [67,68]. Within Cytoscape 3.10.3, networks were laid out using force-directed or organic layouts; node size was scaled by degree centrality. Topological measures (degree, betweenness) were computed via built-in analysis tools.

2.12.7. GO and KEGG Pathway Analysis Using ShinyGO

Intersecting targets were submitted to ShinyGO (https://bioinformatics.sdstate.edu/shinygo/, accessed on 4 June 2025) [71,72] with organism set to Homo sapiens. Enrichment analyses for Gene Ontology categories (biological process, molecular function, cellular component) and KEGG pathways were performed, applying FDR-adjusted $p < 0.05$ as the significance cutoff. The PI3K-Akt signaling pathway, a potential mechanism by which the polyphenols may modulate hypertrophy-related processes [73–75], was analyzed. Top GO terms and KEGG maps were exported for summary figures and integrated with network findings.

2.12.8. Enrichment Analysis via Metascape

To complement ShinyGO results, shared targets were also analyzed in Metascape (https://metascape.org/) [76–78] with the organism set to human. An express analysis was employed, using $p < 0.05$ to identify Gene Ontology analysis categories found in the Metascape and collected enrichment GO analysis results.

3. Results

3.1. Analysis of Methanolic Extract of Rauwolfia serpentina by HPLC-DAD

A validated HPLC method has been developed to evaluate the linearity, accuracy, stability, and precision of 16 polyphenolics. The method effectively identifies and quantifies these polyphenolics in the ethanolic root extract of *R. serpentina* within 45 min. Figure 1 shows the polyphenols in the extract separated by chromatography. The content of each phenolic compound in the *R. serpentina* root extract was estimated using the relevant calibration curve, and the results were displayed as the average of five measurements (Table 2).

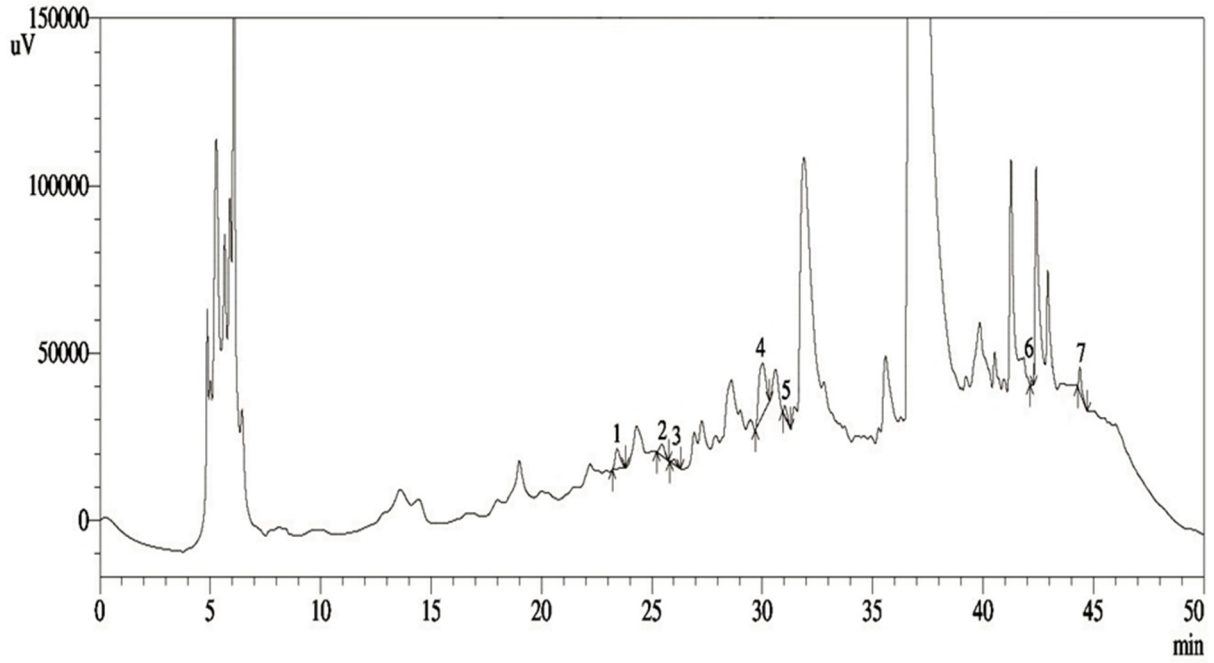

Figure 1. HPLC chromatogram of ethanol extract of *R. serpentina*. Peaks: 1, catechol; 2, vanillic acid; 3, syringic acid; 4, rutin hydrate; 5, *p*-Coumaric acid; 6, quercetin; 7, kaempferol.

Table 2. Phenolic antioxidants present in the *Rauwolfia serpentina* extract.

Name of Standard	*Rauwolfia serpentina* (Sorpogondha) (mg/100 g of Dry Extract)
3,4 Dihydroxy benzoic acid	ND
Gallic acid	ND
Catechol	24.29 ± 0.09
Catechin hydrate	ND

Table 2. *Cont.*

Name of Standard	*Rauwolfia serpentina* (Sorpogondha) (mg/100 g of Dry Extract)
(−) Epicatechin	ND
Caffeic acid	ND
Vanillic acid	6.34 ± 0.07
Syringic acid	1.64 ± 0.10
Rutin hydrate	70.22 ± 0.31
Trans-Ferulic acid	ND
p-Coumaric acid	2.79 ± 0.04
Rosmarinic acid	ND
Quercetin	0.88 ± 0.02
Myricetin	ND
Kaempferol	5.50 ± 0.15
Trans-Cinnamic acid	ND

Note: ND = Not Detected.

3.2. The Impact of Rauwolfia serpentina on Total Heart, LV, and RV of Heart-Wet Weights and Kidney-Wet Weights

Figure 2A shows the various groups' moist weights of the kidneys and heart. In comparison to the control rats, the ISO-induced rats' total heart weight was considerably greater ($p < 0.05$) (Figure 2A). The total cardiac wet weight of rats treated with *R. serpentina* root extract plus isoprenaline was lower ($p < 0.05$) than that of rats treated with isoprenaline (Figure 2A). In addition, *R. serpentina* root extract resulted in a normal total heart wet weight ($p < 0.05$) in control rats when compared to the isoprenaline group (Figure 2A).

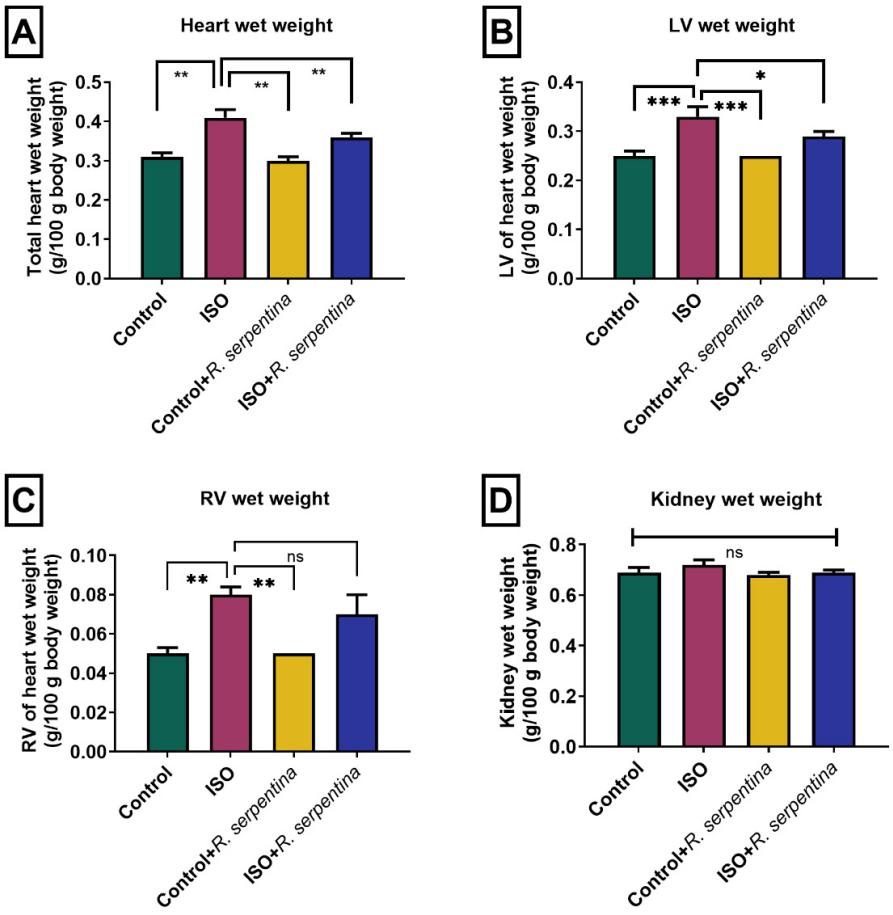

Figure 2. Effect of *R. serpentina* root extract on (**A**) total heart wet weight; (**B**) LV heart wet weight (**C**) RV heart wet weight, and (**D**) kidney wet weights in ISO administered rats. The values, n = 6, are displayed as mean ± SEM. Using GraphPad Prism Software (version 9), a one-way ANOVA and the Tukey multiple comparisons test were performed for analysis. Findings are deemed non-significant when $p > 0.05$ and significant when $p < 0.05$. Asterisk marks are * $p < 0.05$; ** $p < 0.01$; and *** $p < 0.001$.

Rats given isoprenaline had a considerably higher left ventricle (LV) of the heart-wet weight than the control group ($p < 0.05$) (Figure 2B). On the other hand, rats treated with *R. serpentina* root extract and given isoprenaline had a lower LV of heart wet weight ($p < 0.05$) than rats given isoprenaline alone (Figure 2B). Furthermore, LV of cardiac moist weight was lower in control rats treated with *R. serpentina* ($p < 0.05$) than in rats given isoprenaline (Figure 2B).

Similar findings were shown by the RV of heart wet weights, which increased when isoprenaline was administered in comparison to the control group ($p < 0.05$) (Figure 2C). However, in rats given isoprenaline, treatment with *R. serpentina* root extract substantially decreased the RV of heart-wet weight ($p < 0.05$) (Figure 2C). Interestingly, the RV of heart-wet weight did not change significantly between animals provided isoprenaline and control rats treated with *R. serpentina* root extract ($p > 0.05$) (Figure 2C).

The ISO group as well as the control group did not vary significantly in kidney wet weight ($p > 0.05$) (Figure 2D). Relative to the ISO category, the wet kidney weight of rats treated with *R. serpentina* did not change ($p > 0.05$) (Figure 2D). Additionally, animals given isoprenaline and control rats treated with *R. serpentina* root extract did not vary significantly ($p > 0.05$) in kidney wet weight (Figure 2D).

3.3. The Impact of Rauwolfia serpentina on a Variety of Biomarkers Identified in the Plasma of Rats Given Isoprenaline

Administration of ISO leads to heart and kidney dysfunction, as evidenced by elevated plasma levels of biomarkers associated with heart and impaired renal function, such as uric acid, CK-MB, and creatinine. In our study, we observed a significant increase ($p < 0.05$) in cardiac CK-MB in rats administered with ISO compared to the control group (Figure 3A). Rats treated with *R. serpentina* root extract and given ISO exhibited significantly lower CK-MB activity ($p < 0.05$) in plasma compared to rats given ISO alone (Figure 3A). Furthermore, CK-MB activity was reduced in control rats treated with *R. serpentina* ($p < 0.05$) compared with those given isoprenaline (Figure 3A).

Plasma concentrations of renal dysfunction markers, including creatinine and uric acid, can increase with ISO treatment and indicate kidney impairment. Rats given ISO in this study had markedly higher levels of uric acid and creatinine ($p < 0.05$) relative to the control group. (Figure 3B,C). The administration of *R. serpentina* root extract resulted in a substantial ($p < 0.05$) decrease in creatinine and uric acid levels in rats given ISO ((Figure 3B,C). Relative to the ISO group, uric acid and creatinine concentrations in the control group were demonstrated to be reduced ($p < 0.05$) by the root extract of *R. serpentina* ((Figure 3B,C).

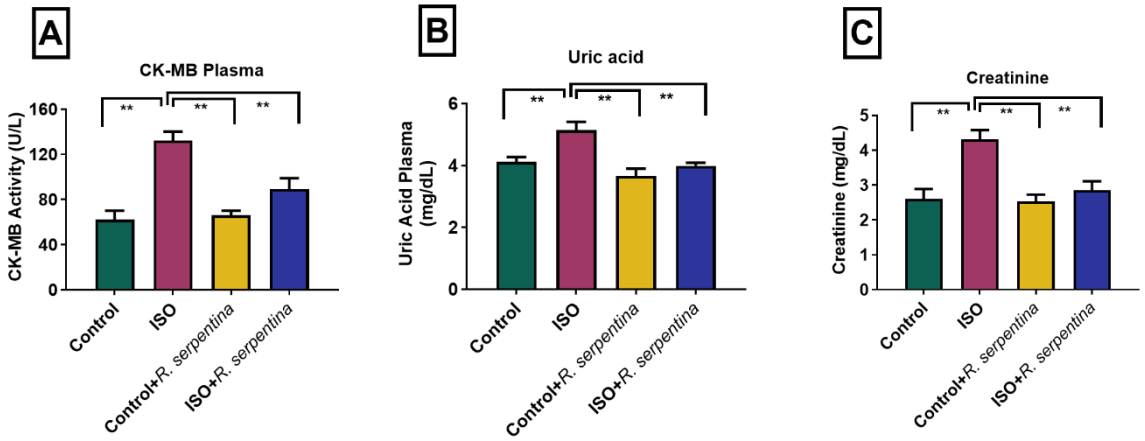

Figure 3. Effect of *Rauwolfia serpentina* root extract on CK-MB, uric acid, and creatinine in ISO administered rats. The values are shown as mean ± SEM, n = 6. GraphPad Prism Software, version 9, was used for analysis, and a one-way ANOVA along with Tukey multiple comparisons test were performed. A significance level of $p < 0.05$ is applied to the results. Asterisk marks are ** $p < 0.01$.

3.4. The Impact of Rauwolfia serpentina on Oxidative Stress Markers

In the study we conducted, we investigated the impact of *R. serpentina* on oxidative stress in rats treated with isoprenaline by measuring markers such as NO, MDA, AOPP, and MPO in plasma, heart, and renal homogenates.

Our findings revealed a noticeable increase ($p < 0.05$) in malondialdehyde biosynthesis, a byproduct of lipid peroxidation, in the hearts, kidneys, and plasma of rats administered ISO, contrasting with the control group

(Figure 4A–C). However, rats treated with *R. serpentina* root extract and isoprenaline showed a decrease in MDA ($p < 0.05$) in heart, kidney, and plasma homogenates compared with rats administered isoprenaline alone (Figure 4A–C). Additionally, in the control group, *R. serpentina* root extract reduced MDA levels ($p < 0.05$) compared with the isoprenaline group (Figure 4A–C).

Additionally, when juxtaposed with the control rats, the shot of ISO resulted in an abrupt increase in the amount of NO in the kidney, heart, and plasma ($p < 0.05$) (Figure 4D–F). Treatment with *R. serpentina* normalized the NO levels ($p < 0.05$) in the heart, kidney, and plasma of ISO-administered rats (Figure 4D–F). Meanwhile, compared with ISO-treated rats, control rats receiving *R. serpentina* therapy showed lower NO levels in heart and kidney homogenates and plasma (Figure 4D–F).

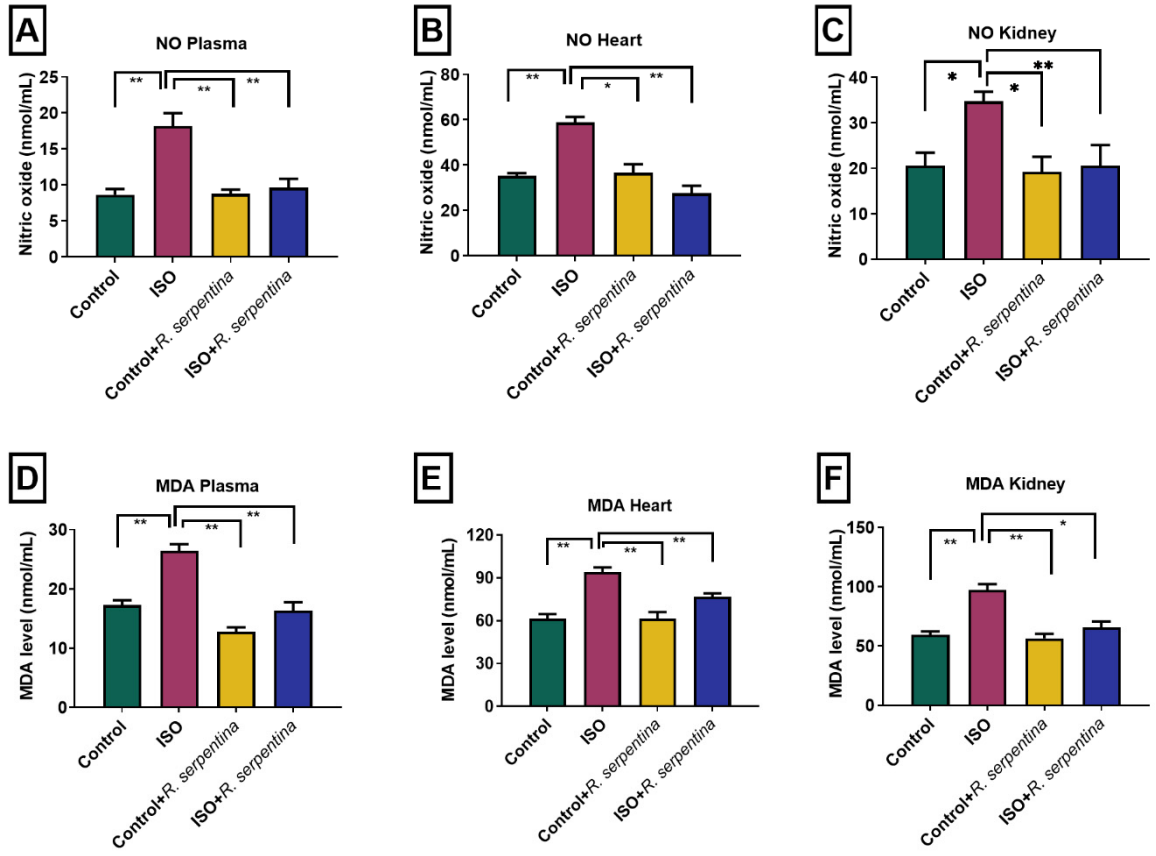

Figure 4. Effect of *R. serpentina* root extract on oxidative stress indicators in rats offered ISO. Considering n = 6, values are listed as mean ± SEM. Tukey's multiple comparisons test and one-way ANOVA were used for analysis, and GraphPad Prism software, version 9, was used. The significance level for the outcomes is set at $p < 0.05$. Asterisk marks are * $p < 0.05$ and ** $p < 0.01$.

In this phase of our research, we observed a significant increase in AOPP levels in rats given isoprenaline ($p < 0.05$) compared with the control group (Figure 5A–C). However, when rats were treated with both *R. serpentina* root extract and isoprenaline, there was a noticeable decrease in AOPP levels ($p < 0.05$) in plasma, heart, and kidney homogenates compared to rats that received isoprenaline alone (Figure 5A–C). Furthermore, in the control group, *R. serpentina* root extract reduced AOPP levels ($p < 0.05$) compared with the isoprenaline-treated group (Figure 5A–C).

MPO levels in rats were significantly increased ($p < 0.05$) after subcutaneous ISO administration compared to the control group (Figure 5D,E). Treatment with *R. serpentina* root extract and isoprenaline resulted in a decrease ($p < 0.05$) in MPO levels in heart and kidney tissues compared to the isoprenaline-administered rats (Figure 5D,E). *R. serpentina* treatment in control rats also led to a decreased MPO activity ($p < 0.05$) compared to rats administered with isoprenaline (Figure 5D,E).

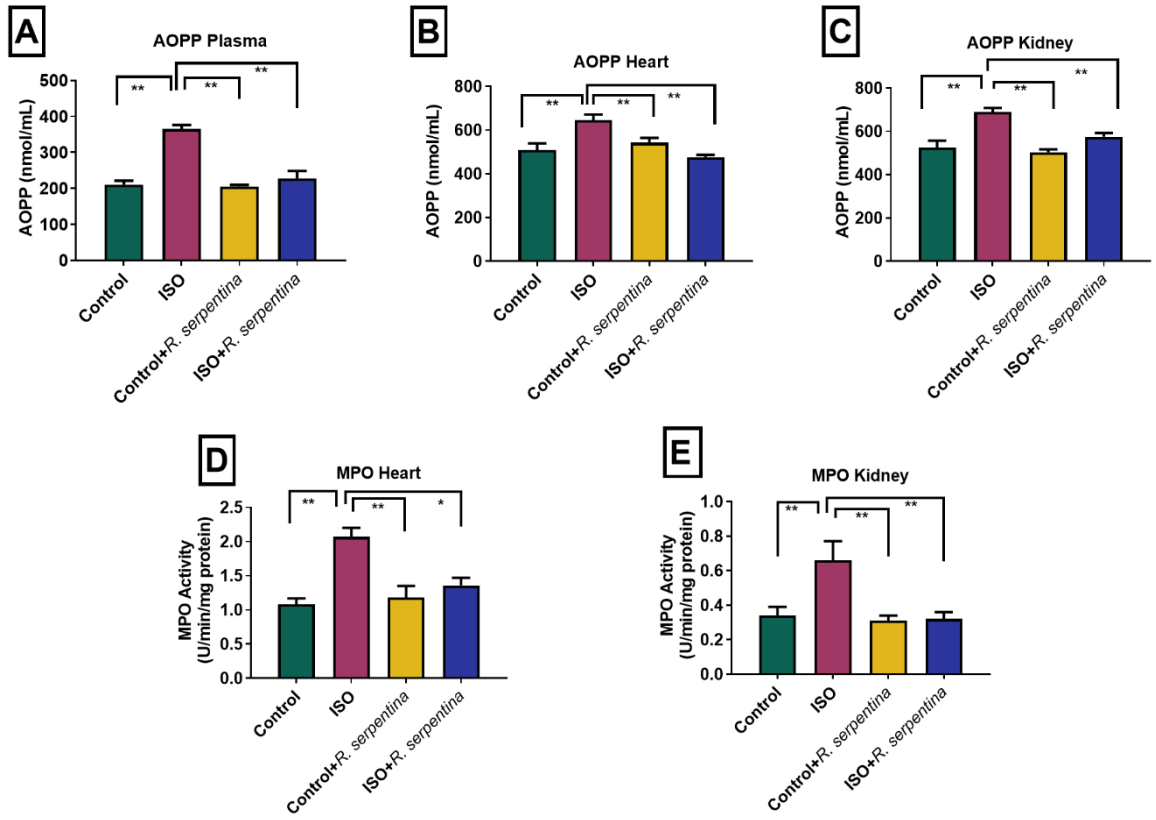

Figure 5. Effect of *R. serpentina* root extract on oxidative stress indicators in ISO administered rats. The values, n = 6, are displayed as mean ± SEM. Utilizing Graph Pad Prism Software, version 9, a one-way ANOVA and a Tukey multiple comparisons test were performed for analysis. At $p < 0.05$, the results are deemed significant. Asterisk marks are * $p < 0.05$ and ** $p < 0.01$.

3.5. Effects of Rauwolfia serpentina on Antioxidant Enzyme Activities

Our study revealed that rats treated with isoprenaline showed significantly lower levels of SOD relative to the control group ($p < 0.05$) (Figure 6A–C). However, when rats were administered *R. serpentina* extract along with isoprenaline, there was a substantial spike in SOD activity ($p < 0.05$) in plasma, heart, and kidney tissues (Figure 6A–C). Additionally, the *R. serpentina* extract demonstrated a significant reduction ($p < 0.05$) in the levels of SOD in plasma, cardiac, and renal homogenates, contrasting with the ISO group (Figure 6A–C).

Furthermore, this section of the study found that rats administered isoprenaline exhibited significantly lower catalase activity in the heart, kidney, and plasma ($p < 0.05$) compared with the control group (Figure 6D–F). Conversely, rats treated with *R. serpentina* root extract showed significantly restored catalase activity ($p < 0.05$) compared to those administered with ISO (Figure 6D–F). Moreover, the control group showed increased catalase activity ($p < 0.05$) compared with the ISO-treated group after receiving *R. serpentina* root extract (Figures 6D–F and 7).

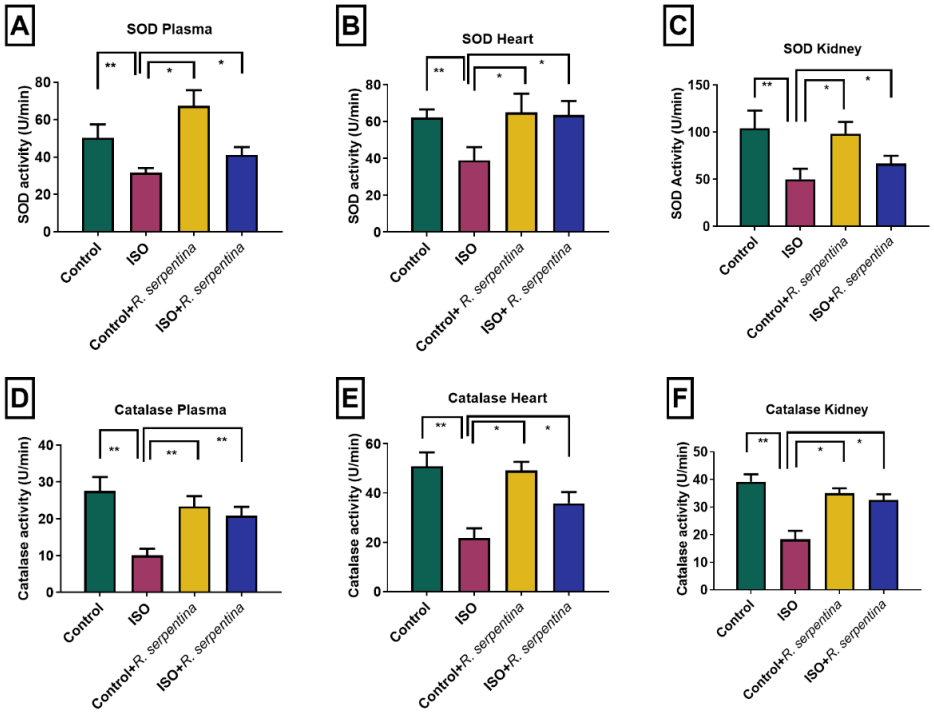

Figure 6. Effect of *R. serpentina* root extract on antioxidant enzymes activities in ISO administered rats. GraphPad Prism Software, version 9, was used for the analysis, which included a one-way ANOVA and a Tukey multiple comparisons test. The results are shown as mean ± SEM, n = 6. At $p < 0.05$, the results are deemed significant. Asterisk marks are * $p < 0.05$ and ** $p < 0.01$.

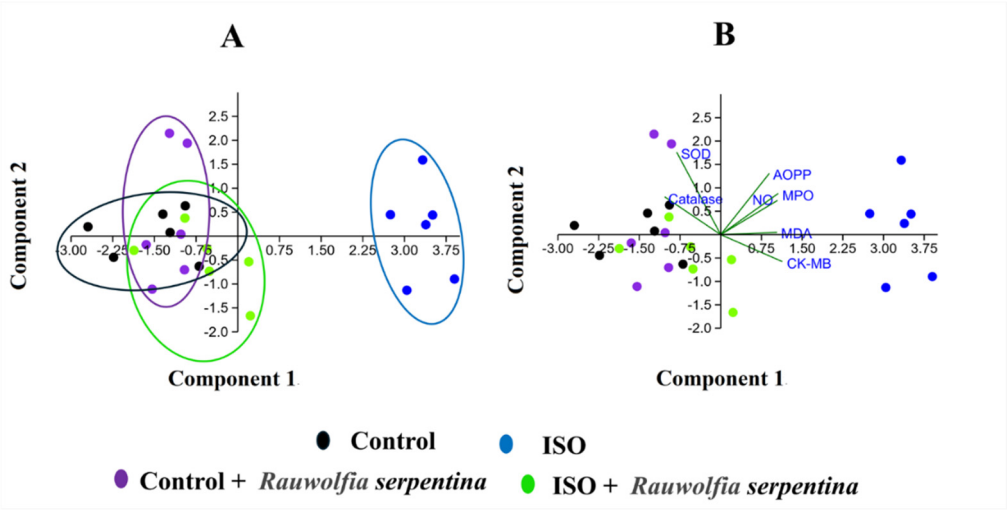

Figure 7. Principal component analysis (PCA) biplot graph of biochemical parameters of the heart in various groups. (**A**) PCA score plot showing clustering of samples from four experimental groups: Control (black), ISO-treated (blue), Control + Rauwolfia serpentina (purple), and ISO + Rauwolfia serpentina (green). The plot displays separation of groups based on the first two principal components (Component 1 and Component 2), which represent the major sources of variation in the dataset. The ISO group is distinctly separated from the control group along Component 1, indicating significant biochemical alterations induced by isoproterenol treatment. The ISO + Rauwolfia serpentina group clusters between the ISO and control groups, suggesting partial restoration toward the normal biochemical profile following treatment with Rauwolfia serpentina. Ellipses represent the clustering tendency of each group. (**B**) PCA loading plot illustrating the contribution of measured variables to the separation observed in the score plot. Oxidative stress and cardiac injury markers such as CK-MB, MDA, MPO, AOPP, and NO are oriented toward the ISO group, indicating their association with ISO-induced cardiac damage. In contrast, antioxidant enzymes including SOD and catalase are oriented toward the control and treated groups, reflecting their contribution to antioxidant defense. Together, the PCA demonstrates that Rauwolfia serpentina treatment mitigates ISO-induced oxidative stress and cardiac injury by shifting the biochemical profile closer to the control condition.

3.6. Effect of R. serpentina on Expression of Antioxidant Genes Heart in Isoprenaline (ISO) Administered Rats

In this phase of our research, we examined gene expression of antioxidant and anti-inflammatory enzymes by RT-PCR, which are primarily regulated by the nuclear factor erythroid 2-related factor 2 (Nrf-2), a versatile protein with cytoprotective properties. Administration of ISO in rats resulted in a change in Nrf-2 levels. Compared to the control rats, the transcript level was vastly reduced in rats provided ISO ($p < 0.05$) (Figure 8A). As it turned out, the inducible as well as constitutive isoforms of heme oxygenases (i.e., HO-1 and HO-2) were also substantially lower in the rats treated with ISO. Nevertheless, as opposed to the isoprenaline group, supplementation with *R. serpentina* root extract notably ($p < 0.05$) boosted these genes (Figure 8A–C). Additionally, the oral consumption of *R. serpentina* root extract was also observed to improve the gene expressions of enzymes that fight oxidative stress, including catalase, glutathione peroxidase (GPx), and SOD (Figure 8D–F).

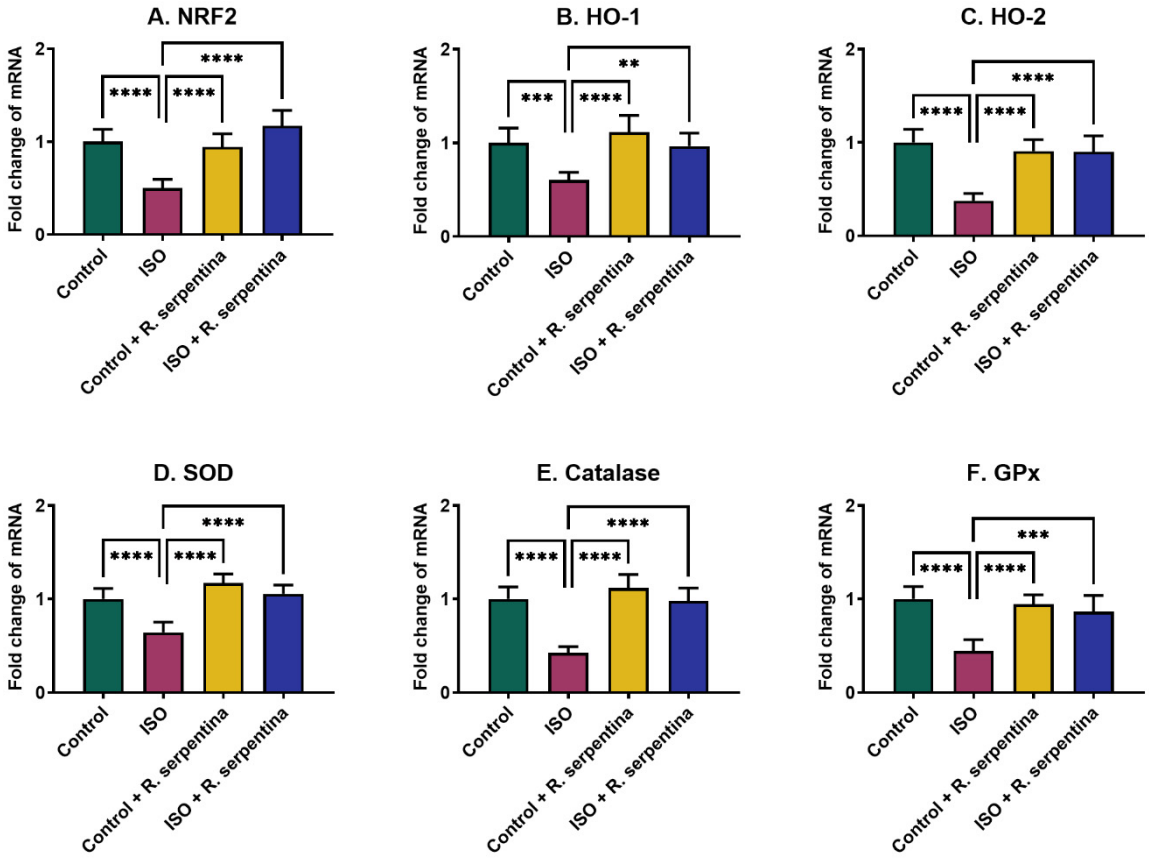

Figure 8. Effect of *R. serpentina* root extract on relative expressions of antioxidant genes in ISO-administered rats. GraphPad Prism Software, version 9, was used for the analysis, which included a one-way ANOVA and a Tukey multiple comparisons test. The results are shown as mean ± SEM, n = 6. At $p < 0.05$, the results are deemed significant. Asterisk marks are ** $p < 0.01$; *** $p < 0.001$; and **** $p < 0.0001$.

3.7. Effect of R. serpentina on Gene Expressions of Inflammatory Mediators

The transcription factor that regulates the expression of pro-inflammatory mediators such as TNF-α, IL-1, NF-κB, IL-6, and iNOS was quantified to assess the effectiveness of *R. serpentina* root extract in suppressing inflammation and fibrosis induced by isoprenaline. Likewise, TGF-β gene expression was also investigated. The expression of these genes was significantly elevated ($p < 0.05$) in heart tissue of rats after isoprenaline administration compared with control rats (Figure 9A–F). Treatment of *R. serpentina* extract dramatically ($p < 0.05$) suppressed the expression of these genes at the transcript level (Figure 9A–E). However, the ISO group did not significantly vary from the control group in its expression of NF-κB ($p > 0.05$) (Figure 9F).

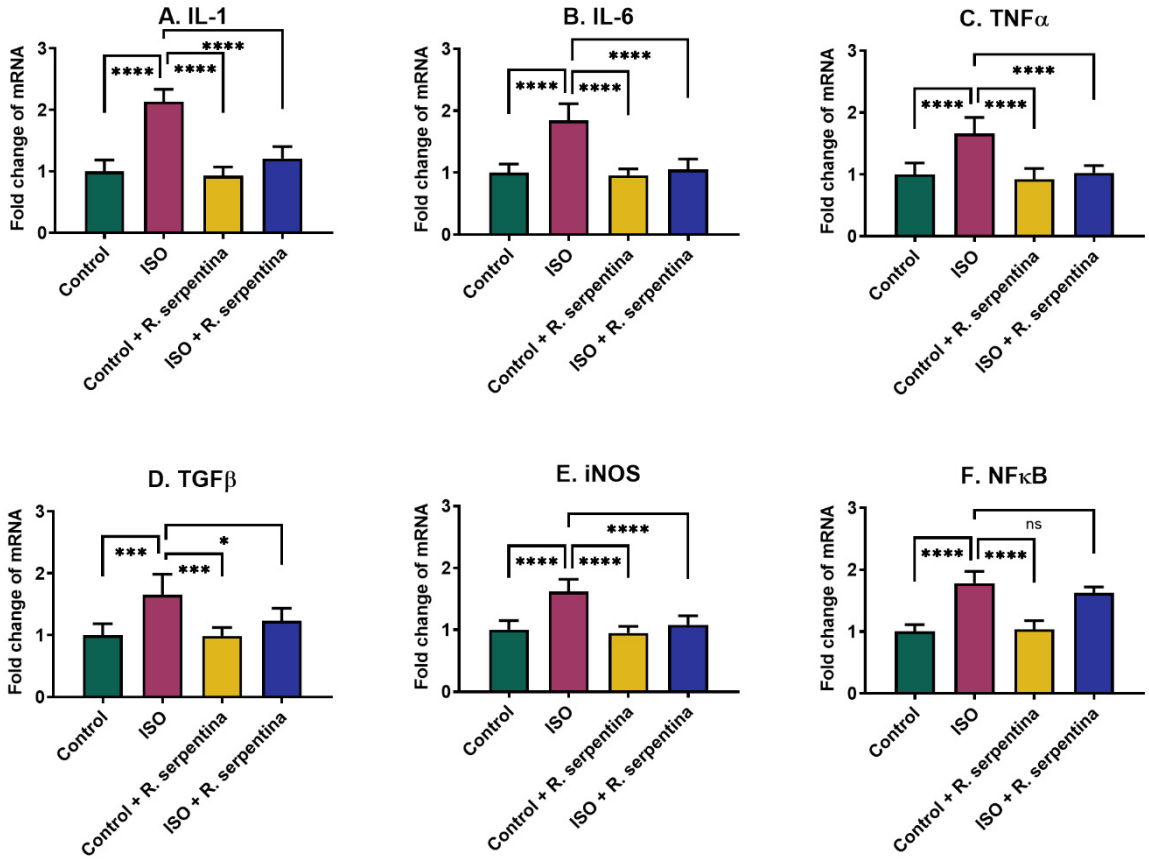

Figure 9. Effect of *R. serpentina* root extract on relative expressions of inflammation-related genes in ISO-administered rats. GraphPad Prism Software, version 9, was used for the analysis, which included a one-way ANOVA and a Tukey multiple comparisons test. The results are shown as mean ± SEM, n = 6. At $p < 0.05$, the results are deemed significant. Asterisk marks are * $p < 0.05$; *** $p < 0.001$; and **** $p < 0.0001$.

3.8. Impact of Rauwolfia serpentina upon Histological Alterations in the Hearts of Rats Given Isoprenaline

In the hearts of the control group, no evidence of necrosis, edema, or inflammation was observed, and the histoarchitecture appeared intact and consistent (Figure 10A). The hearts of the control+ *R. serpentina* group displayed intact and homogeneous histoarchitecture, free of edema, necrosis, and inflammation, which aligned with the control group's findings (Figure 10C). As opposed to the control category, the hearts of rats administered with isoprenaline exhibited significant inflammatory cell infiltration, along with necrosis of muscle fibers, heightened extracellular matrix accumulation, and edema (Figure 10B). Rats administered with isoprenaline and treated with *R. serpentina* demonstrated protection from cardiac injury, as evidenced by reduced inflammatory cell infiltration, necrosis, and edema compared to the isoprenaline category (Figure 10D).

The histological analysis of the control group revealed normal distribution and alignment of collagen in the heart's left ventricle (Figures 10E and 11A). Rats in the control group and those fed with *R. serpentina* exhibited similar lower levels of collagen deposition in the heart tissues (Figures 10G and 11C). Conversely, rats administered with isoprenaline showed a significant increase in collagen accumulation and fibrosis, unlike the control group (Figures 10F and 11B). Notably, treatment with *R. serpentina* markedly mitigated the collagen content and fibrosis induced by isoprenaline in the rats (Figures 10H and 11D).

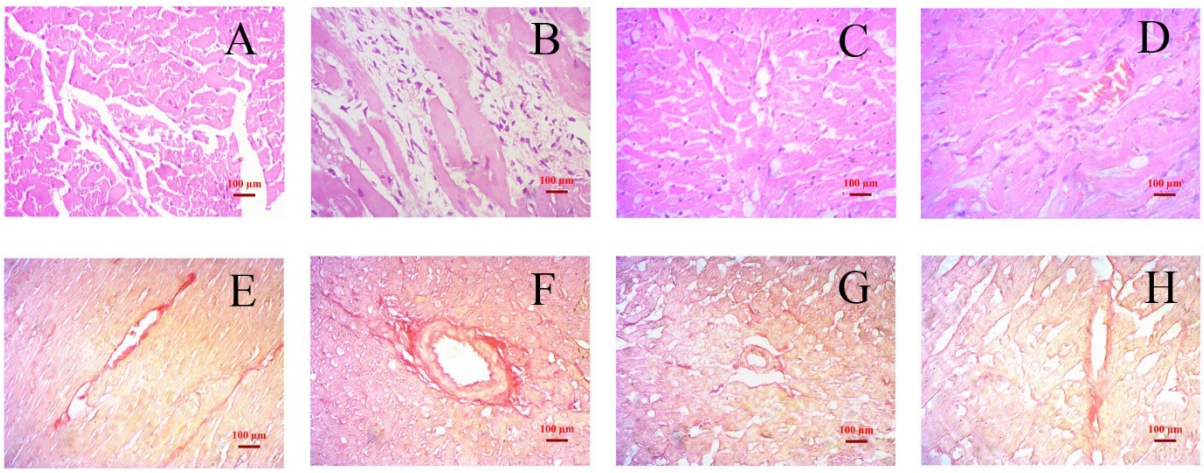

Figure 10. Effect of *R. serpentina* root extract on mono-nuclear inflammatory cell infiltration in the heart of ISO-administered rats. (**A**) Control (H&E staining); (**B**) ISO (H&E staining); (**C**) Control + *R. serpentina* (H&E staining); (**D**) ISO + *R. serpentina* (H&E staining); (**E**) Control (Sirius red staining); (**F**) ISO (Sirius red staining); (**G**) Control + *R. serpentina* (Sirius red staining); (**H**) ISO + *R. serpentina* (Sirius red staining). Magnification ×40 (Axioscope, Zeiss).

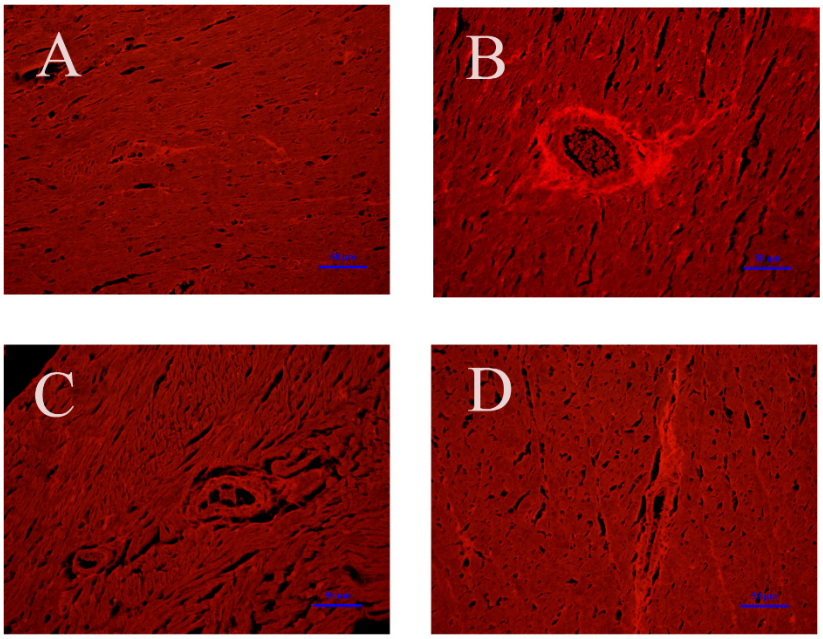

Figure 11. Effect of *R. serpentina* root extract on fibrosis in the heart of ISO-administered rats. Fluorescence microscopy picture (**A**) Control (Sirius red staining); (**B**) ISO (Sirius red staining) (**C**) Control + *R. serpentina* (Sirius red staining); (**D**) ISO + *R. serpentina* (Sirius red staining). Magnification ×20 (Leica DM 1000 coupled with a camera Model: FLEXACAM C3).

3.9. Impact of Rauwolfia serpentina upon Histological Alterations in the Kidneys of Rats Given Isoprenaline

In the control group, the H&E staining of kidney segments revealed a standard structure for the glomerulus and the tubules (Figure 12A). Both the Control + RS group and the control group exhibited similar structural features (Figure 12C). Administration of ISO resulted in parenchymal cell changes, glomerular congestion, and tubular hypertrophy in various kidney regions (Figure 12B). However, these structural abnormalities observed in rats given ISO were alleviated by administering *R. serpentina* extract (Figure 12D). Normal collagen deposition was demonstrated in control rats by staining with Sirius red (Figure 12E). Both the Control + RS group and the control group exhibited comparable structural features (Figure 12G). Conversely, rats treated with ISO showed

increased collagen content and fibrosis in kidney sections (Figure 12F). Isoprenaline-treated rats improved less than the *R. serpentina* treatment group (Figure 12H).

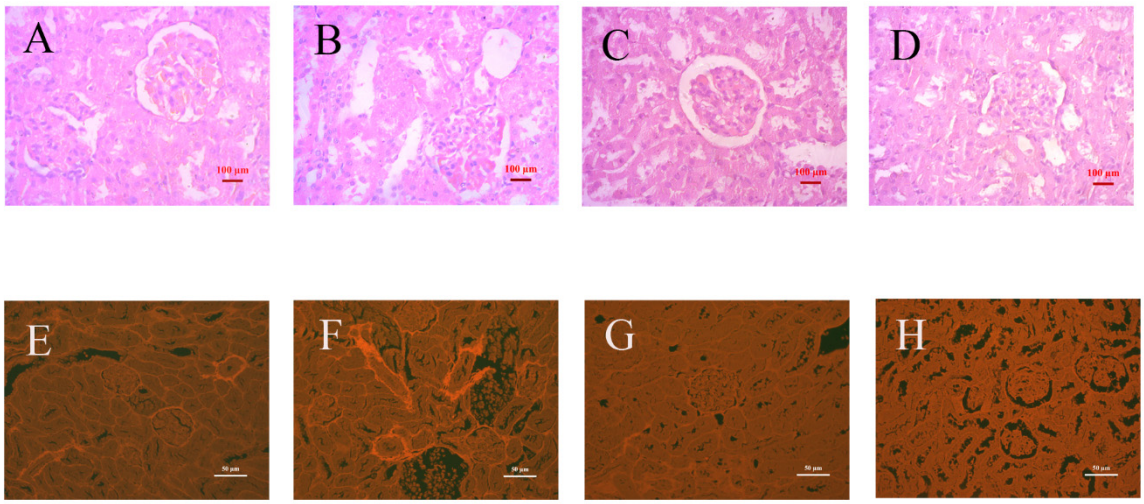

Figure 12. Effect of *R. serpentina* root extract on kidney infiltration of inflammatory cells and collagen accumulation in ISO-administered rats. Upper Panel- (**A**) Control (H&E staining); (**B**) ISO (H&E staining); (**C**) Control + *R. serpentina* (H&E staining); (**D**) ISO + *R. serpentina* (H&E staining), Magnification ×40 (Axioscope, Zeiss). Lower Panel; (**E**) Control (Sirius red staining); (**F**) ISO (Sirius red staining); (**G**) Control + *R. serpentina* (Sirius red staining); (**H**) ISO + *R. serpentina* (Sirius red staining), Magnification ×20 (Leica DM 1000 coupled with a camera Model: FLEXACAM C3).

Network Pharmacology of *R. serpentina*

For understanding the multi-target, multi-pathway therapeutic processes of complex natural products in the treatment of diseases is made possible through network pharmacology, a revolutionary systems biology method that combines computational prediction with experimental validation [79]. Network pharmacology is a new way of looking at drug discovery and development that incorporates system-level analysis of therapeutic interventions with several components and targets, rather than the old “one drug, one target” method [80]. This technology combines computational target prediction, database mining, network design, and pathway analysis to clarify the intricate molecular mechanisms of natural product therapies[81].

Using a combination of computational databases, this study found 141 shared targets between disease-associated genes and compound-specific molecular targets, as well as six significant polyphenols from *R. serpentina* that have potential as cardiac hypertrophy treatments (Figure 13). To further the development of evidence-based medications and to build reasonable frameworks for the discovery of cardiovascular drugs from natural product sources, it is crucial to understand these multi-target therapeutic networks.

In order to reduce prediction bias in single-database approaches and guarantee complete coverage, the use of numerous computational databases for target prediction represents the current best practices in network pharmacology research [82]. Target datasets for cardiac hypertrophy and *R. serpentina* polyphenols were robustly created using the complete target analysis, which effectively combined several computational databases [80,81]. The identification of cardiac hypertrophy targets employed GeneCards and OMIM databases, resulting in 175 unique disease-associated targets [58,83–86]

For the target prediction major 6 polyphenols of *R. serpentina* found in our study, we have used several databases BATMAN-TCM [49], SuperPred by Charité [50], TargetNet [53], Way2Drug[54], and sea search [56]. BATMAN-TCM (Bioinformatics Analysis Tool for Molecular Mechanism of Traditional Chinese Medicine) functions as a dedicated platform for predicting the targets of traditional Chinese medicine compounds utilizing similarity-based algorithms and literature mining[80,81]. SuperPred, developed by Charité, is a validated web server for target prediction utilizing structural similarity and machine learning methodologies[87]. The prediction accuracy was further improved through the integration of experimental data and varied algorithmic approaches using the TargetNet, Way2Drug, and Similarity ensemble approach (SEA) search databases[82,88,89]. A total of 4760 predicted molecular targets of these 6 polyphenols of *R. serpentina* were identified from these databases.

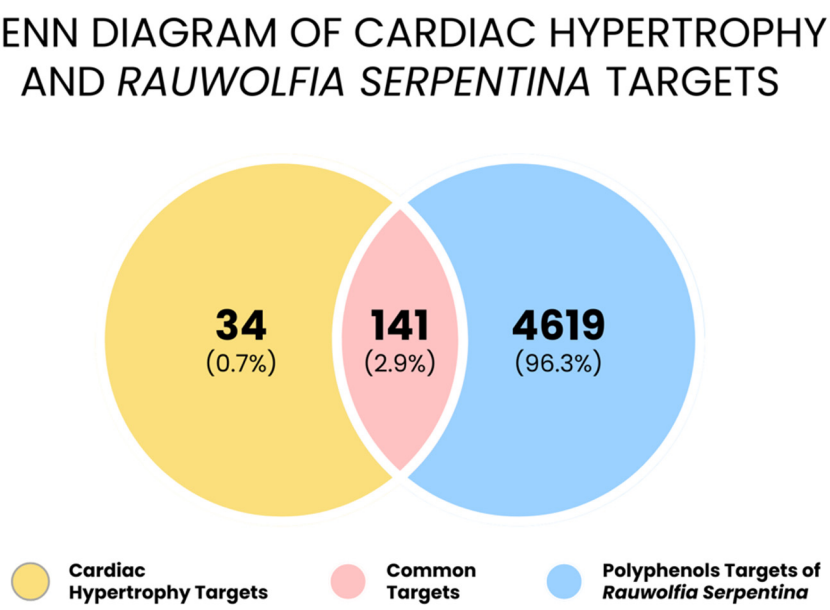

Figure 13. Venn diagram analysis of target overlap between cardiac hypertrophy and *R. serpentina* polyphenols.

The Venn diagram analysis revealed three distinct target populations with significant implications for understanding the therapeutic mechanisms of *R. serpentina* polyphenols in cardiac hypertrophy. The critical therapeutic intersection comprised 141 common targets (2.9% of total targets), representing molecular pathways where polyphenol compounds directly engage cardiac hypertrophy-associated mechanisms (Files S2 and S3). The targets specific to cardiac hypertrophy included 34 genes, accounting for 0.7% of the total targets, which represent molecular pathways associated with the disease that are not directly influenced by the polyphenol compounds [90,91]. The polyphenol-specific targets included 4619 molecular targets, representing 96.3% of the total targets, thereby highlighting the significant molecular interaction potential of *R. serpentina* polyphenolic compounds [73,92].

The observed target overlap indicates that the conventional cardiovascular applications of *R. serpentina* are founded on authentic molecular interactions, rather than being attributable to placebo effects or non-specific activities [92].

The merged network of network pharmacology analysis of *R. serpentina* is visualized using Cytoscape 3.10.3. Cytoscape is a prominent open-source platform utilized for the analysis and visualization of complex networks, commonly applied in systems biology and network pharmacology research [67,93]. The developed network demonstrated a complex therapeutic system comprising multiple components and targets, involving six principal polyphenols derived from *R. serpentina* in relation to cardiac hypertrophy (Figure 14). The network consisted of 148 nodes, including 6 polyphenolic compounds (File S4), one disease phenotype, and 141 protein targets, interconnected by various validated interactions. This network topology illustrates the "many-to-many" relationship inherent in traditional medicinal plants, wherein multiple bioactive compounds concurrently influence various therapeutic targets [93–95].

Visualization using Cytoscape showed highly connected network modules and hub proteins, which likely play key roles in modulating the polyphenolic compounds' cardioprotective effects [77,96]. The 141 shared protein targets identified via integration of the UniProt database encompass a variety of biological pathways essential for the development and progression of cardiac hypertrophy [97]. The protein targets include various functional categories such as transcription factors, kinases, receptors, and signaling molecules that play roles in cardiac remodeling processes [98]. Molecular mechanisms of the cardioprotective effects of *R. serpentina* polyphenols were found through network analysis, which identified highly-connected hub proteins at the center of the therapeutic network as potential intervention and biomarker targets in the treatment of cardiac hypertrophy [77,97,99].

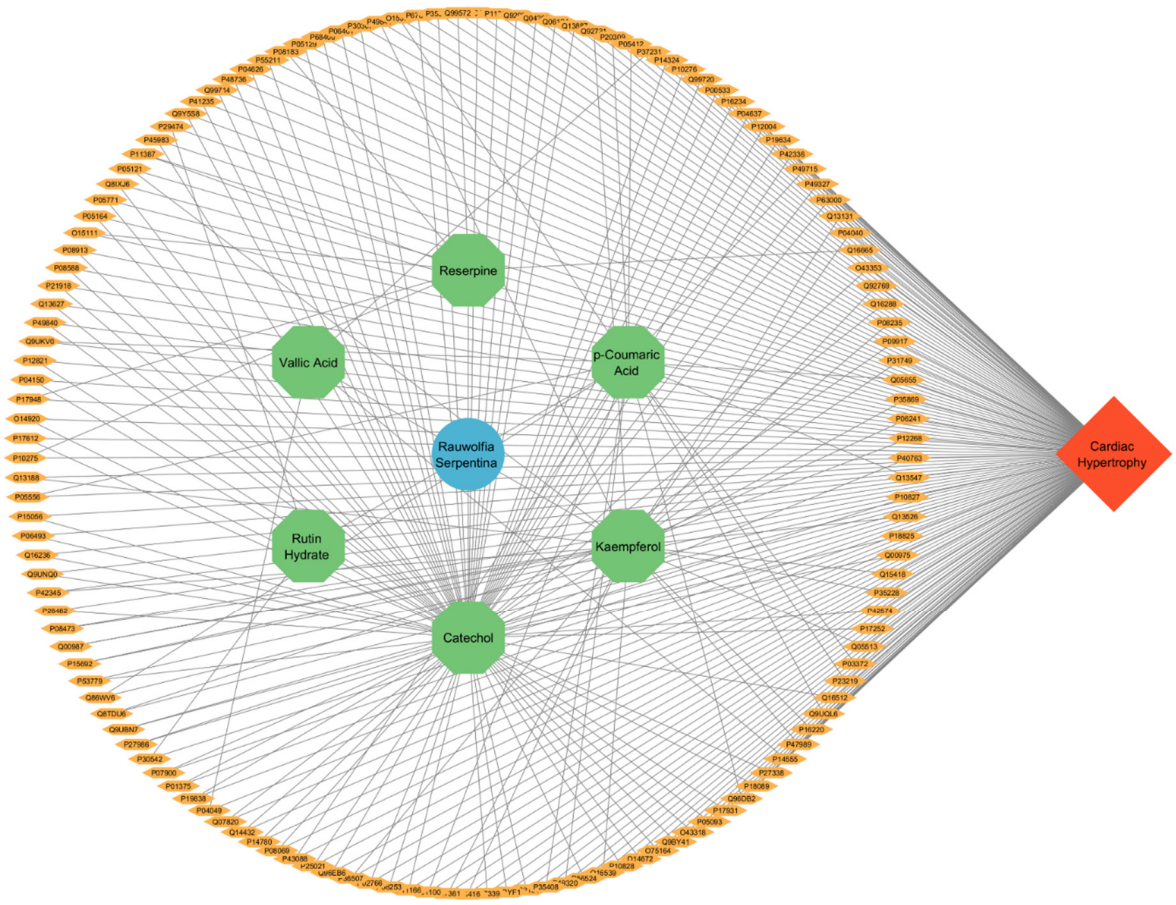

Figure 14. *R. serpentina* merged network. Network pharmacology analysis of *R. serpentina* polyphenols and cardiac hypertrophy. The network visualization displays the complex interactions between six major polyphenols from *R. serpentina* (green hexagons) and cardiac hypertrophy (red diamond) through 141 shared protein targets (orange hexagons). The central polyphenolic compounds include Reserpine, Vanillic Acid, *p*-Coumaric Acid, Rutin Hydrate, Kaempferol, and Catechol.

Network pharmacology predictions are consistent with experimental evidence from recent studies that demonstrate the cardioprotective effects of *R. serpentina* compounds [27]. More recent research has shown that *R. serpentina* drugs have broader therapeutic potential via several molecular targets. Numerous bioactive compounds derived from *R. serpentina* have been discovered by molecular docking investigations to possess inhibitory properties against PARP-1, VEGFR-2, and aldose reductase, three important therapeutic targets [100]. The findings corroborate the multi-target therapeutic approach identified through network pharmacology analysis [101].

Functional annotation of target proteins indicated enrichment in PI3K/AKT signaling, MAPK pathways, inflammatory cascades, and apoptosis regulation, which aligns with the pathophysiology of cardiac hypertrophy and highlights the therapeutic relevance of *R. serpentina* polyphenols across multiple pathways [97,98,102].

Protein-protein interaction networks are essential biological systems that regulate cellular activities, disease processes, and therapeutic reactions by means of intricate molecular interactions[103]. Critical insights for the development of evidence-based cardiovascular therapeutics and advancements in precision medicine approaches in cardiac disease management were derived from this extensive protein-protein interaction (PPI) network analysis, which utilized Cytoscape 3.10.3 for network topology analysis and the STRING database with default parameters for human proteins to characterize the molecular interactions among 141 shared protein targets between *R. serpentina* polyphenols and cardiac hypertrophy (Figure 15) [69,104]

The STRING database integrates experimentally validated and computationally predicted associations, scored by confidence and multiple evidence sources like experimental data, text mining, genomic context analysis, and co-expression to build protein interaction networks [69,105]. Protein-Protein Interaction analysis is further done with the help of Cytoscape, an open-source platform designed for complex network analysis and visualization in systems biology and network pharmacology, which offers tools for network construction, topological analysis, and pathway visualization, utilizing centrality measures such as degree, betweenness, and closeness to evaluate the significance of proteins within biological networks quantitatively [67,106,107].

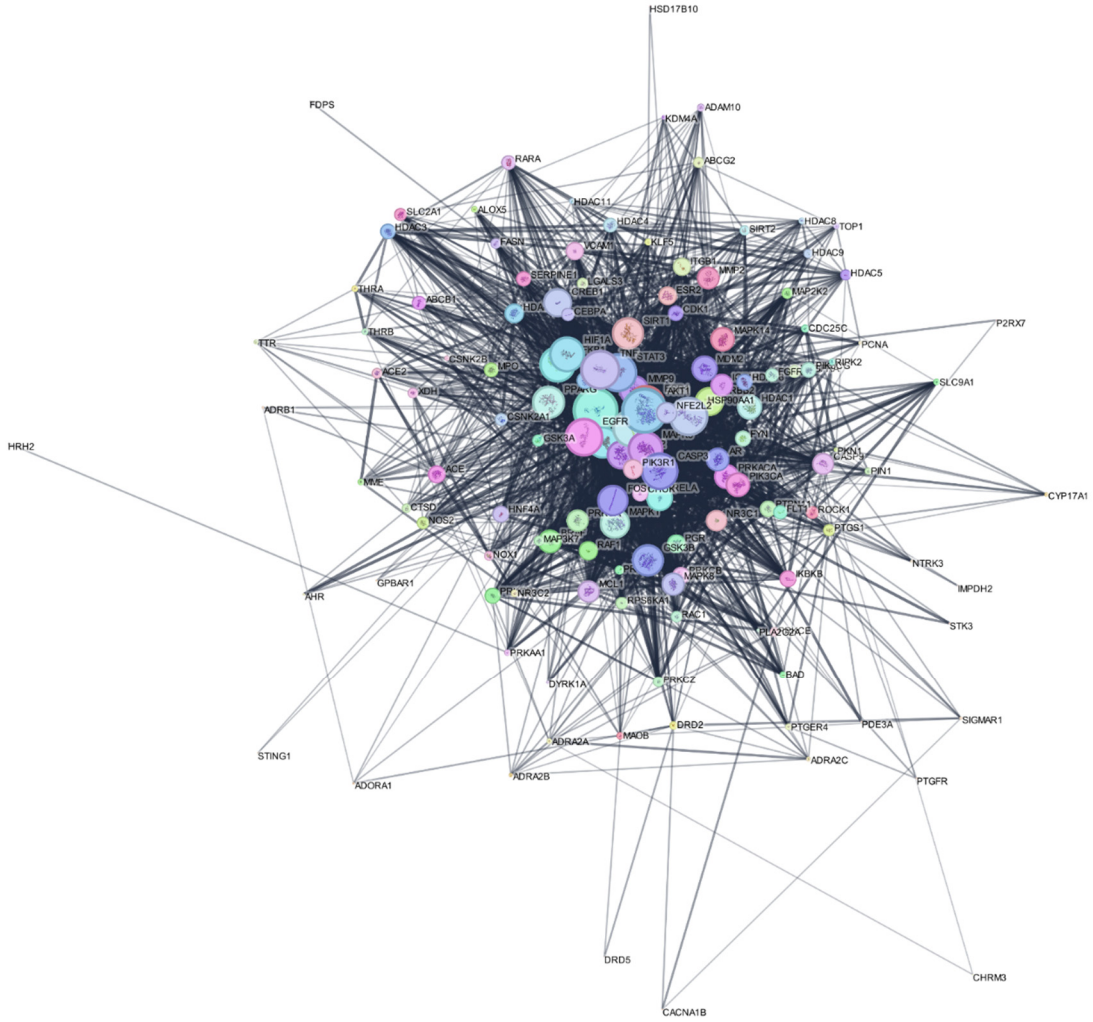

Figure 15. Protein-Protein Interaction Network analysis of 141 shared targets between *R. serpentina* polyphenols and cardiac hypertrophy. The PPI network analysis effectively established a complex molecular interaction system involving 141 shared protein targets between *R. serpentina* polyphenols and cardiac hypertrophy, utilizing the STRING database with default parameters [69,105].

The analysis using Cytoscape 3.10.3 demonstrated notable heterogeneity in protein connectivity, with degree centrality varying from 5 to 102 connections per protein, as given in Table 3 below. The analysis of network topology revealed several key hub proteins exhibiting significantly high centrality measures across various parameters. Network centrality measures are graph-theoretic metrics that quantify the relative importance of individual nodes in complex networks, based on their structural positions and connectivity patterns[108–111]. Betweenness centrality measures the degree to which a node is situated on the shortest paths connecting other pairs of nodes within a network, reflecting its function as a bridge or intermediary in network communication[112]. Closeness centrality quantifies the efficacy of a node in communicating with the entire network by measuring its proximity to all other nodes [109]. These can be found in Supplementary Materials (File S1).

Table 3. The Protein-Protein Interaction Network for *Rauwolfia serpentina.*

Protein Name	Degree	Betweenness Centrality	Closeness Centrality
AKT1	102	0.078121069	0.791907514
TP53	101	0.060399853	0.782857143
TNF	88	0.048119089	0.728723404
HSP90AA1	87	0.040732091	0.728723404
ESR1	86	0.03982232	0.724867725
STAT3	86	0.021880319	0.724867725
JUN	86	0.019289496	0.717277487
EGFR	85	0.035242945	0.721052632
CASP3	83	0.023478206	0.706185567
NFKB1	80	0.013680111	0.691919192

Table 3. *Cont.*

Protein Name	Degree	Betweenness Centrality	Closeness Centrality
MAPK3	79	0.021043542	0.691919192
HIF1A	79	0.015832114	0.695431472
PPARG	73	0.023609357	0.678217822
SIRT1	71	0.021044117	0.674876847
GSK3B	71	0.017682781	0.671568627
MTOR	71	0.013647124	0.668292683
FOS	69	0.010385644	0.661835749
MAPK1	67	0.012399058	0.652380952
MMP9	66	0.007472804	0.646226415
PTGS2	64	0.022040573	0.643192488
CREB1	64	0.01054924	0.646226415
ERBB2	64	0.011069366	0.643192488
RELA	59	0.007080404	0.625570776
MDM2	58	0.007621275	0.625570776
PRKACA	55	0.021683445	0.619909502
HDAC1	55	0.010814273	0.614349776
MAPK14	54	0.006275782	0.611607143
PIK3CA	54	0.005695194	0.60619469
AR	52	0.007837775	0.60619469
BRAF	52	0.004622504	0.608888889
MAPK8	51	0.003675071	0.60619469
MMP2	50	0.002785926	0.598253275
IGF1R	50	0.003950869	0.595652174
MCL1	49	0.004505592	0.595652174
PRKCA	49	0.011693983	0.598253275
CASP9	48	0.014801233	0.595652174
NR3C1	47	0.006616585	0.598253275
NFE2L2	47	0.002448223	0.593073593
PIK3R1	44	0.003866241	0.578059072
HDAC2	43	0.004864962	0.575630252
RAF1	42	0.004703721	0.578059072
ESR2	41	0.006840483	0.573221757
PGR	41	0.002418925	0.575630252
VCAM1	40	0.001415815	0.573221757
ITGB1	40	0.002756087	0.570833333
ACE	39	0.006723588	0.575630252
PRKCB	38	0.009752272	0.570833333
NOS3	38	0.001633742	0.570833333
IKBKB	37	0.002014469	0.570833333
HNF4A	37	0.001664188	0.559183673
HDAC6	36	0.001683991	0.56147541
PTPN11	36	0.002019951	0.563786008
CHUK	35	0.000936293	0.563786008
FYN	35	0.001137743	0.556910569
PRKCD	35	0.006809889	0.55465587
CDK1	34	0.002006542	0.552419355
HDAC3	34	0.002946213	0.545816733
PIK3CG	34	0.002942344	0.559183673
SERPINE1	33	0.001192973	0.55465587
RARA	32	0.001818179	0.550200803
HDAC4	32	0.00113334	0.550200803
MPO	32	0.001298058	0.552419355
ABCB1	31	0.000703395	0.55465587
FLT1	31	0.000422052	0.548
FGFR1	30	0.001517025	0.550200803
CEBPA	29	0.000726431	0.543650794
ROCK1	28	0.00145221	0.528957529
SLC2A1	28	0.000329569	0.543650794
CSNK2A1	28	0.001847941	0.539370079
PDGFRA	28	0.000355292	0.541501976

Table 3. *Cont.*

Protein Name	Degree	Betweenness Centrality	Closeness Centrality
RPS6KA1	27	0.001616026	0.543650794
NOS2	27	0.000281084	0.539370079
GSK3A	26	0.000922054	0.537254902
PTGS1	26	0.010498323	0.537254902
RAC1	25	0.001460539	0.53515625
LGALS3	25	0.000368649	0.53515625
HDAC5	24	0.001332518	0.531007752
PRKCZ	24	0.000878167	0.53515625
MAP2K2	24	0.000524079	0.53515625
ABCG2	24	0.000455064	0.526923077
ACE2	23	0.000460378	0.528957529
XDH	23	0.000936817	0.53515625
FASN	23	0.016527183	0.531007752
MAP3K7	23	0.000819175	0.528957529
SIRT2	22	0.000873291	0.518939394
NOX1	21	0.00017018	0.524904215
PRKCE	20	0.008610895	0.513108614
HDAC9	20	0.000381781	0.516981132
PRKCG	20	0.002231641	0.5
CTSD	20	0.000581204	0.524904215
DRD2	18	0.015859834	0.516981132
ADAM10	17	0.000192396	0.513108614
CDC25C	17	0.001264572	0.513108614
MAOB	16	0.009294559	0.518939394
NR3C2	16	0.000614391	0.513108614
BAD	15	0.000105389	0.501831502
PIN1	15	0.000445619	0.491039427
KLF5	15	3.19087×10^{-5}	0.50929368
PRKAA1	14	0.014885176	0.503676471
HDAC8	14	0.000153424	0.501831502
RIPK2	14	4.10925×10^{-5}	0.494584838
THRB	14	0.00080818	0.501831502
SLC9A1	14	0.000368003	0.503676471
MME	14	0.000280031	0.507407407
ALOX5	14	0.00035891	0.5
PTGER4	14	0.001955905	0.513108614
THRA	14	0.000376838	0.492805755
TOP1	13	0.000572799	0.491039427
HDAC11	12	2.04461×10^{-5}	0.480701754
ADRA2A	12	0.00278289	0.447712418
CSNK2B	11	0.000203893	0.482394366
TTR	10	0.000317808	0.482394366
ADRA2C	10	0.000454255	0.446254072
KDM4A	9	1.95146×10^{-5}	0.485815603
PKN1	9	0.000185741	0.482394366
CYP17A1	9	0.00010535	0.482394366
ADRA2B	9	0.000295412	0.422839506
PCNA	8	0.000297623	0.467576792
DYRK1A	7	3.06692×10^{-6}	0.485815603
PLA2G2A	7	4.23934×10^{-5}	0.465986395
SIGMAR1	7	0.00245111	0.482394366
NTRK3	6	0	0.456666667
AHR	5	0	0.462837838
ADORA1	5	0.00018366	0.46440678
ADRB1	5	0.000221342	0.470790378

The application of centrality measures to the *R. serpentina* protein network in a systematic way simplifies the process of discovering cardiovascular drugs by allowing for target prioritization based on centrality and a multi-target, synergistic approach that mimics the pharmacology of traditional medicinal plants through the coordinated modulation of important molecular targets [113–116].

From Table 3, The analysis of network topology within the cardiac hypertrophy interactome identified AKT1 as the central hub (degree = 102, betweenness = 0.078, closeness = 0.792) [117,118], with TP53 closely following (degree = 101, betweenness = 0.060, closeness = 0.783)[119,120]. TNF has been identified as a significant central node, with a degree of 88, a betweenness of 0.048, and a closeness of 0.729 [117,119]. The eight proteins, including HSP90AA1, ESR1, STAT3, JUN, and EGFR, which demonstrate high degree, betweenness, and closeness centrality, form the core regulatory network that drives the pathogenesis of cardiac hypertrophy [121–123].

Metascape is an online platform that integrates more than 40 separate knowledge bases, allows users to perform functional enrichment analysis on gene lists, and simplifies the Express Analysis interface for comparative analyses across various experiments [76]. Metascape's integration of multiple databases, including KEGG, Reactome, WikiPathways, and Gene Ontology, facilitates comprehensive and cross-validated functional enrichment analyses, effectively clarifying the therapeutic mechanisms of *R. serpentina* polyphenols [76,124].

The enrichment analysis of 141 shared protein targets between *R. serpentina* polyphenols and cardiac hypertrophy identified 20 highly significant terms ($-\log_{10} P \approx 30–50$), with the most notable being Pathways in cancer (hsa05200), Gastrin signaling (WP4659), and Cellular response to hormone stimulus (GO:0032870) (Figure 16) [76].

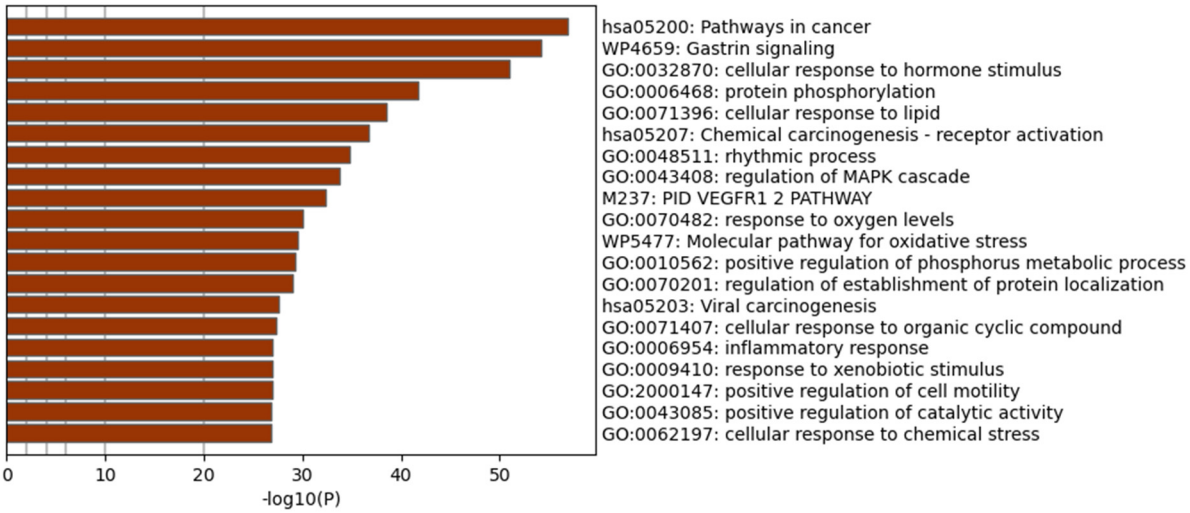

Figure 16. Enrichment heatmap for *R. serpentina* polyphenols targets in cardiac hypertrophy.

Color-coded Metascape GO enrichment of 141 shared *R. serpentina* polyphenol targets across biological process, molecular function, and cellular component domains reveals multi-level modulation underpinning evidence-based cardiovascular applications and guiding standardized formulation and drug discovery (Figure 17) [73,125–127].

The identification of cancer-related pathways as the most significantly enriched category corresponds with the established cardioprotective and anti-inflammatory properties of polyphenolic compounds, given that numerous cellular processes associated with cancer progression intersect with those involved in cardiac hypertrophy pathogenesis. The significant enrichment of hormone response pathways corroborates the traditional application of *R. serpentina* in managing cardiovascular conditions, wherein hormonal signaling is pivotal in cardiac remodeling processes [128,129].

DisGeNET, a comprehensive platform compiles gene–disease associations from literature, expert repositories, and genome-wide studies[130]. In contrast, Metascape combines DisGeNET with functional enrichment, interactome analysis, and annotation from various knowledge bases to facilitate rapid large-scale interpretation of gene lists [76].

According to the Figure 18, the DisGeNET enrichment analysis through Metascape of 141 common targets related to *R. serpentina* polyphenols and cardiac hypertrophy indicated significant associations ($P < 10^{-10}$ for most conditions) with 20 pathologies, dominated by diabetic complications, cardiovascular/cerebral disorders, neural pathologies, and neoplasms. The extreme significance ($-\log_{10}(P)$ up to 60) underscores robust mechanistic links between these targets and multiorgan diseases. Links to diabetic cardiomyopathy, renal hypertension, and cerebrovascular disease expand therapeutic and safety considerations.

The findings establish a comprehensive framework for experimental targeting, biomarker identification, and the development of translational strategies in evidence-based natural product cardiovascular therapeutics.

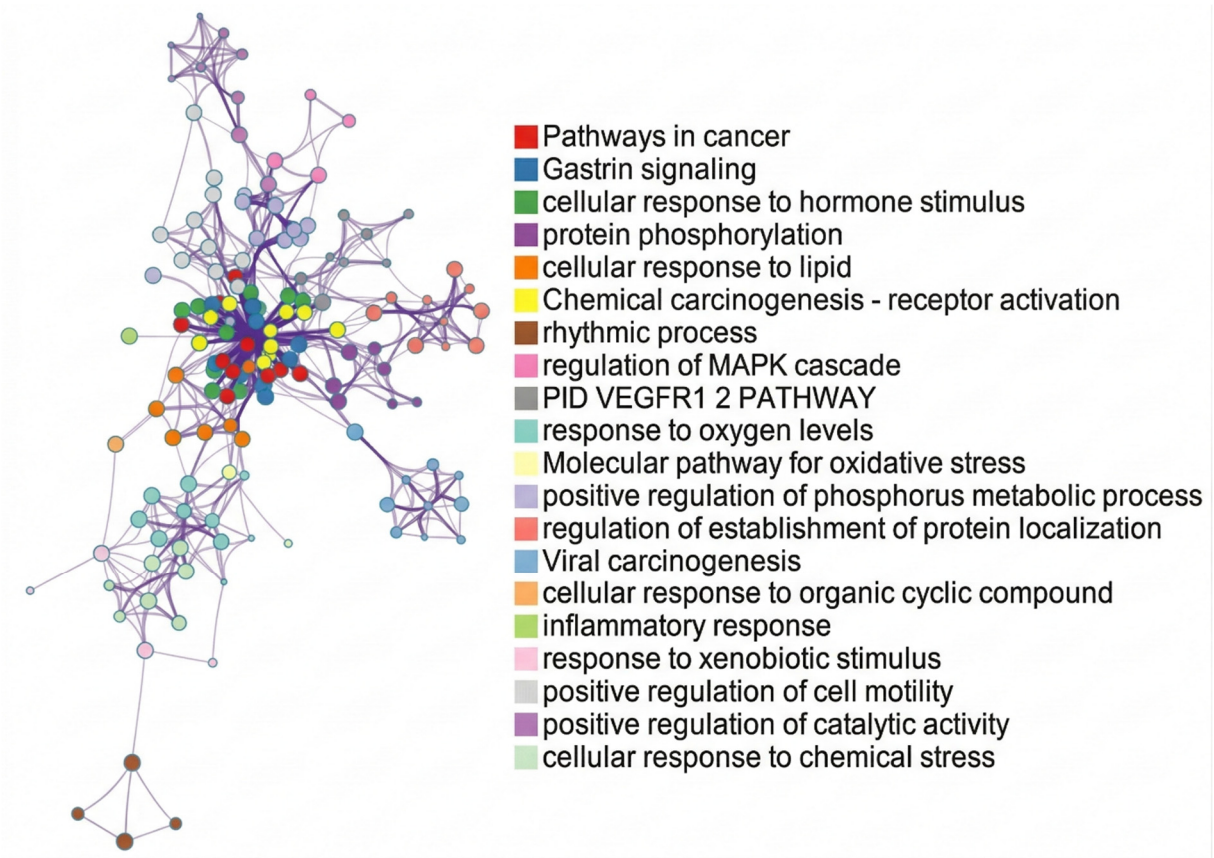

Figure 17. Enrichment GO analysis for *R. serpentina* polyphenols using Metascape.

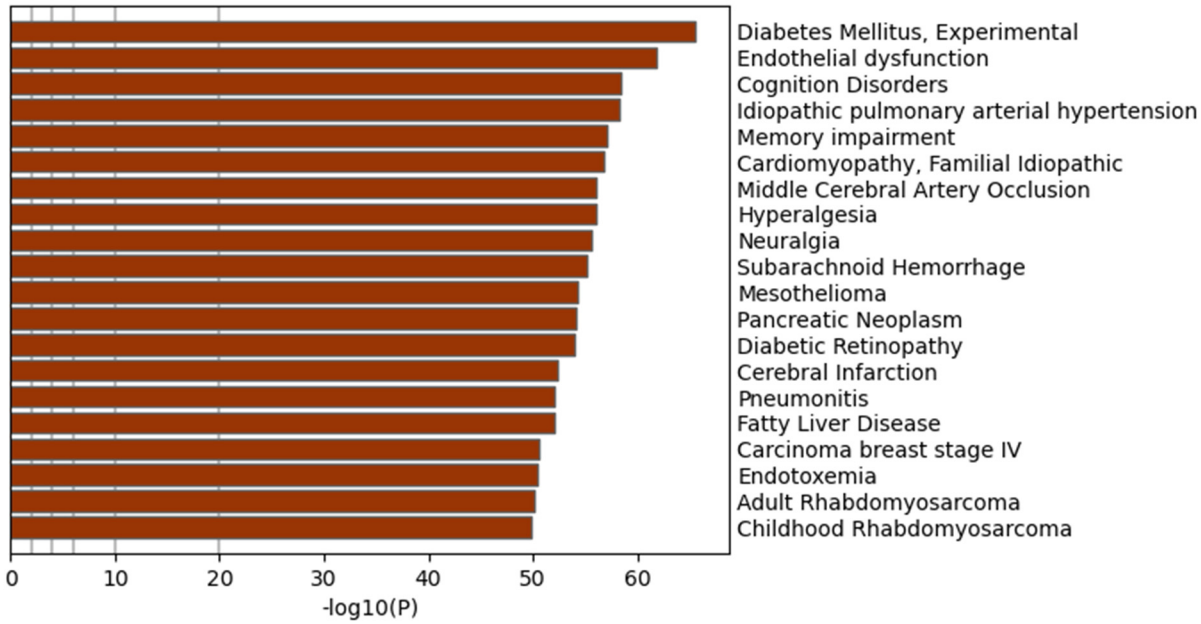

Figure 18. Summary of enrichment analysis in DisGeNET using metascape for *R. serpentina* polyphenols.

The PI3K/AKT pathway serves as a key regulator of cardiomyocyte growth, survival, metabolism, and hypertrophic responses [131,132]. Utilized ShinyGO to map 141 shared protein targets of six *R. serpentina* polyphenols onto the KEGG PI3K/AKT pathway, employing red highlights to denote direct interactions, thus clarifying multi-target therapeutic mechanisms (Figure 19) [71]. ShinyGO is a web-based graphical tool that incorporates KEGG and STRING APIs to deliver interactive pathway diagrams, enrichment statistics, and gene characteristics through an intuitive interface [71].

This pathway analysis sought to identify PI3K/AKT nodes influenced by *R. serpentina* polyphenols, illustrate their multi-target cardioprotective interactions, and facilitate rat model validation, emphasizing the pathway's critical role in cardiac hypertrophy and heart failure prevention.

A total of 141 UniProt-annotated proteins associated with six *R. serpentina* polyphenols (reserpine, vallic acid, p-coumaric acid, rutin, kaempferol, catechol) and cardiac hypertrophy were compiled. KEGG pathway enrichment was conducted using ShinyGO (v0.80) for Homo sapiens, and the PI3K/AKT pathway diagram was retrieved via the KEGG API.

Red highlights on corresponding nodes indicated upstream targeting of growth factor receptors (IGF1R, PDGFRA) and PI3K catalytic subunits (PIK3CA/B), AKT isoforms, and central signaling nodes including AKT1/2/3 and mTOR complex components (mTOR, PRAS40). Additionally, downstream modulation of effectors such as GSK3B, FOXO1/3, and BAD/BCL2 family members was observed, collectively outlining a multi-target cardioprotective network for experimental validation in rat models of cardiac hypertrophy.

IGF1R is a transmembrane tyrosine-kinase receptor that interacts with IGF-1, leading to autophosphorylation and the recruitment of PI3K [133]. Its overexpression in cardiomyocytes promotes "beneficial hypertrophy" through the PI3Kα–AKT signaling pathway [133,134]. PDGFRA, a cell-surface receptor tyrosine kinase activated by PDGF ligands, is crucial for the maintenance of cardiac fibroblasts and adaptive remodeling [135–138]. PIK3CA/B lipid kinases catalyze the conversion of PIP_2 to PIP_3, facilitating the anchoring of AKT, while increased p110α activity provides protection against pressure-overload hypertrophy [122,139]. AKT1/2/3 serine/threonine kinases, activated by PIP_3 binding and PDK1/mTORC2 phosphorylation, enhance cardiomyocyte survival and reduce pressure-overload damage [140–142]. mTORC1, comprising mTOR and PRAS40, detects growth signals to facilitate protein synthesis, with its activation essential for adaptive hypertrophy [140,143]. GSK3B is a constitutively active kinase that inhibits pro-hypertrophic transcription factors and requires inhibition by AKT to facilitate physiological growth [144–146]. FOXO1/3 transcription factors, which are sequestered in the cytoplasm following AKT phosphorylation, play a role in limiting maladaptive hypertrophy and oxidative stress [147,148]. Additionally, the BAD/BCL2 family, through AKT-mediated BAD phosphorylation and BCL2 upregulation, provides protection against apoptosis during hypertrophic stress [149,150].

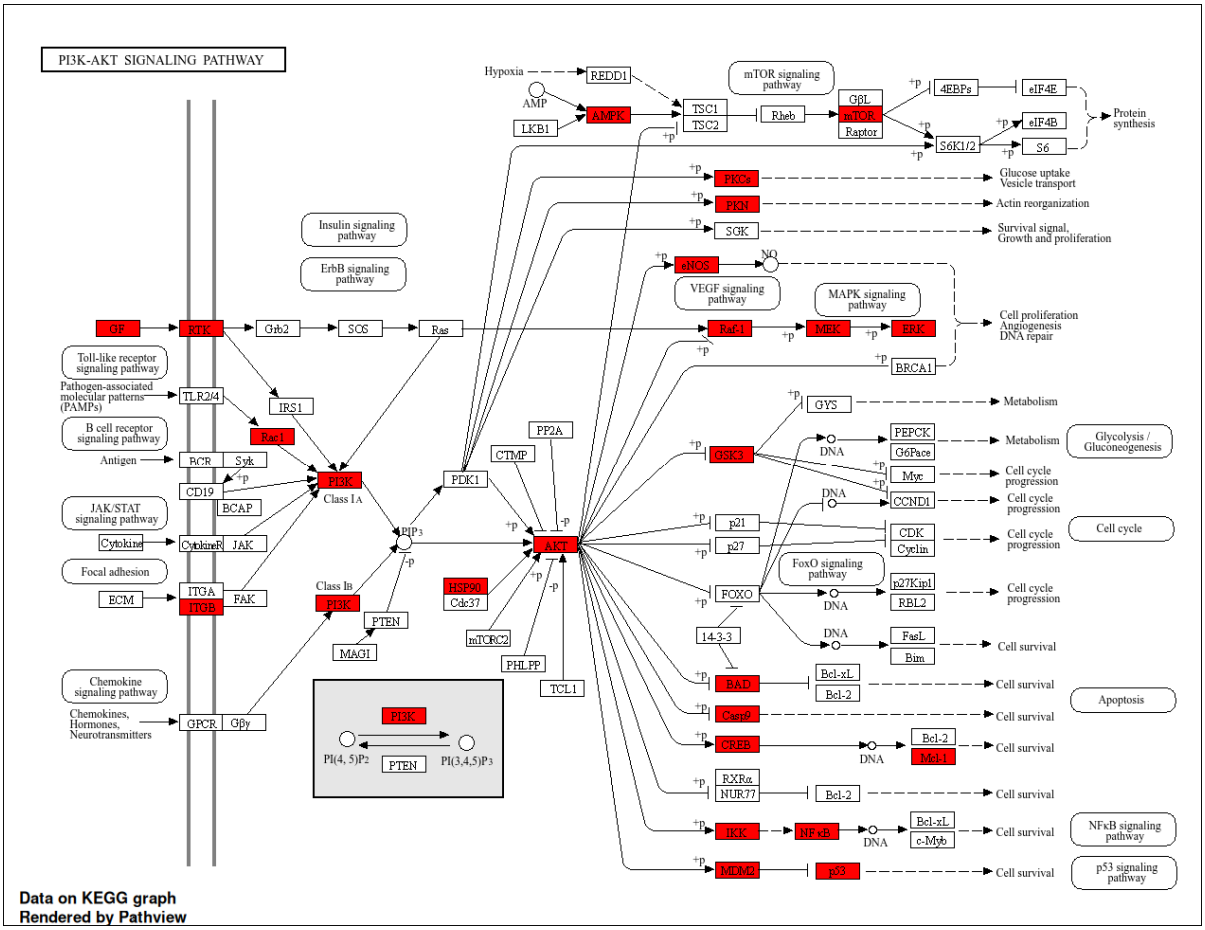

Figure 19. KEGG PI3K signaling pathway associated with *R. serpentina* polyphenols.

4. Discussion

Earlier investigations have shown that antioxidants can reduce the severity of myocardial infarction (MI), slow its progression, and diminish its lingering effects [151]. Antioxidants have also been found to correct oxidative disarray, ameliorate oxidative stress-induced kidney damage, and reduce albuminuria and fibrosis [152]. In this in vivo investigation, rats exposed to an isoprenaline challenge showed a higher cardiac index. The increase in heart weight may be due to excessive water accumulation in the interstitial space, leading to edema. [153]. Even a minor 3.5% rise in the water volume of the myocardium may be linked to a 40% reduction in heart performance [153]. *R. serpentina*, a rich source of antioxidants, could serve as a valuable resource to enhance antioxidant defenses, thereby protecting cells against oxidative stress and maintaining cellular redox balance.

Using high-performance liquid chromatography (HPLC), we successfully identified the specific polyphenolic substances in the ethanol extract of *R. serpentina* and quantified their concentrations. The *R. serpentina* plant contains a variety of polyphenols, including catechols, rutin hydrate, vanillic acid, *p*-coumaric acid, kaempferol, syringic acid, and quercetin, among others. Polyphenols are known for chelating metals and scavenging free radicals in cells, making them potent antioxidants [154]. Our research demonstrated that treatment with *R. serpentina* improved heart and kidney function and structural changes in isoprenaline-treated rats.

Myocardial ischemia leads to damage by suppressing aerobic glucose oxidation, boosting anaerobic glycolysis, and causing an accumulation of lactic acid dehydrogenase [155]. This results in decreased ATP synthesis, disruption of ionic gradients, and deterioration of membrane integrity, potentially leading to the release of enzymes typically contained within cardiomyocytes. Consequently, there is an increase in myocardial enzymes in the bloodstream, and variations in their levels indicate the extent of myocardial ischemia [156]. Our study revealed that rats with AMI exhibited higher CK-MB activity than control rats. Moreover, the root extract of *R. serpentina* reduced cardiac tissue damage and significantly reduced plasma CK-MB activity in rats administered isoprenaline.

Uric acid is the final product of purine metabolism in humans, produced by xanthine oxidase, which also serves as a reservoir of toxic reactive oxygen species (ROS) in the cardiovascular system. It has been implicated in the development of cardiovascular disease [157]. Studies have shown that uric acid can permeate endothelial cells, leading to various pathophysiological effects, including the promotion of oxidative stress, impairment of endothelial function, and reduced nitric oxide [158]. Furthermore, it induces local and systemic inflammation, vascular smooth muscle cell proliferation, and vasoconstriction [159]. Studies have indicated that uric acid is involved in provoking renal inflammation, causing vasoconstriction within the kidneys, and prompting renal failure through the formation of urate crystals [160]. Treatment led to a significant reduction in serum uric acid levels, highlighting the in vivo cardiorenoprotective properties of *R. serpentina*.

Elevated creatinine levels are another factor associated with increased cardiovascular disease risks. Renal impairment is an essential independent indicator of cardiovascular results and death in the overall population following a heart attack as well as heart failure. In individuals who have heart failure, even small increases in creatinine over a specific period, known as worsening renal function (WRF), have been evaluated as an independent prognostic indicator [161]. Isoprenaline significantly increased serum creatinine levels, while treatment with *R. serpentina* notably reduced these levels.

Our study involved measuring the malondialdehyde levels, a byproduct of lipid peroxidation, along with the antioxidant enzyme activity, such as catalase and SOD. Lipid peroxidation is known to play a significant role in myocardial necrosis [162]. Malondialdehyde is recognized as an indicator of lipid peroxidation. Increased peroxidation in chronic kidney disease (CKD) due to oxidative stress can substantially alter cellular structure and function, impairing erythrocyte function. Research has shown higher serum levels of MDA in the erythrocytes of hemodialysis (HD) patients [163]. Our study found that *R. serpentina* reduced the elevation of MDA levels in the heart, kidney, and plasma of rats exposed to isoprenaline. This supports the theory that the potent antioxidant properties of *R. serpentina* contribute to its cardio-reno-protective effects.

Prior research indicates that β-adrenergic stimulation increases iNOS expression, leading to a significant increase in NO production [164]. Many studies have shown that isoprenaline plays a role in the release of cytokines from the myocardium [165], making the inhibition of cytokine production a valuable strategy for reducing myocardial infarction [166]. In our research, we discovered that treatment with *R. serpentina* root extract effectively prevented a decrease in serum and cardiac nitric oxide (NO) levels in rats injected with isoprenaline. Tubular epithelial cells, like endothelial cells, can release substantial amounts of nitric oxide [167]. The observed decrease in kidney NO levels may indicate that *R. serpentina* reduces both ROS and RNS in tubular cells, thereby contributing to its protective benefits by lessening the generation of the highly toxic peroxynitrite.

In our investigation, we focused on AOPP, a well-established marker of oxidative stress used to assess protein oxidation. The interaction of chlorinated oxidants with plasma proteins leads to the production of AOPPs [168].

Studies have revealed that AOPPs inhibit the primary high-density lipoprotein (HDL) receptor [169]. AOPP stimulates the generation of intracellular superoxide via NADPH oxidase, leading to increased superoxide production in various renal cells, including endothelial cells, podocytes, and tubular epithelial cells [170]. Aside from contributing to renal damage, AOPPs are also associated with the development of atherosclerosis and cardiovascular events (CVDs) in CKD [171]. In our study, the introduction of isoprenaline induces protein oxidation in the heart and kidney, but the *R. serpentina* root extract restores it to normal levels.

In our research, we measured the concentration of the essential inflammatory enzyme MPO, which is produced by leukocytes during myeloid differentiation in the bone marrow. Once created, MPO gets stored in primary granules of neutrophils and monocytes, remaining inactive until leukocyte activation and degranulation occur. Increased levels of MPO are related to a more unfavorable prognosis and increased severity of cardiovascular diseases [172]. MPO is responsible for generating free radicals and is responsible for the development of lipid peroxidation and the migration of neutrophils to the site of inflammation [173]. Clinical studies suggest that MPO may contribute to immune-mediated inflammatory syndromes, such as renal disease [174]. The administration of *R. serpentina* to rats exposed to an isoprenaline challenge resulted in a decline in the increase of MPO levels in the kidney and heart.

The roles of redox enzymes, such as SOD and catalase, are crucial in minimizing the harmful effects of oxidative stress by neutralizing free radicals and producing HO• radicals. Enhanced SOD activity has been linked to increased protection against oxidative stress-induced damage. SOD, a potent antioxidant enzyme, transforms superoxide anion radicals ($^{\bullet}O^{-}_{2}$) into hydrogen peroxide (H_2O_2) [175]. Catalase, another essential enzyme, breaks down hydrogen peroxide to maintain optimal levels within the cell, which is crucial for cellular signaling processes [176]. Our research revealed a substantial rise in SOD activity in the group exposed to isoprenaline, indicating that boosting SOD levels could help neutralize superoxide ($^{\bullet}O^{-}_{2}$) radicals and prevent cellular oxidative damage. SOD plays a critical role in regulating steady-state ($^{\bullet}O^{-}_{2}$) levels, which serve as precursors to more harmful derivatives like peroxynitrite or HO•, making it the first line of defense against oxidative stress. Our in vivo findings showed that *R. serpentina* significantly normalized levels of redox enzymes, as indicated by the reversal of changes in SOD and CAT activity in plasma, cardiac, and kidney tissue caused by isoprenaline treatment after *R. serpentina* administration.

Nrf2-mediated gene expression is essential for maintaining cellular balance and shielding tissues from oxidative stress. Nrf-2 triggers the transcription of several critical antioxidative genes that protect against damage, including heme oxygenase-1 (HO-1), superoxide dismutases (SODs), catalase (CAT), and glutathione peroxidase (GPx) [9]. Together, these enzymes form the primary line of defense against ROS-induced tissue injury. For example, HO-1 expression assists the heart by alleviating oxidative stress-induced cardiac injury by breaking down heme and producing protective molecules [177]. Additionally, SODs convert superoxide radicals into hydrogen peroxide, which GPx, along with CAT, further detoxify to prevent cellular damage [9]. In our investigation, it was observed that the consumption of *R. serpentina* root extract to rats with isoprenaline-induced heart damage resulted in an upregulation of crucial antioxidant enzymes, namely SOD, catalase, and GPx. It facilitated the restoration of the Nrf-2-HO1 axis. This outcome aligns with previous studies indicating that antioxidant therapy may help mitigate isoprenaline-induced oxidative stress by influencing the Nrf-2 pathway [178].

When the Nrf-2 protein is elevated, it partially restricts NF-κB activation by generating a reducing environment, thus suppressing the NF-κB transcription factor and explaining the anti-inflammatory impacts of many Nrf2-inducing compounds [179]. Activation of NF-κB after myocardial infarction (MI) and its subsequent translocation to the nucleus triggers the transcription of numerous pro-inflammatory genes, including inflammatory cytokines such as IL-1, TNF-α, and IL-6. This process further amplifies the inflammatory reaction, which causes damage to cardiomyocytes [180]. TNF-α can potentially affect lipid metabolism and plays a crucial role in the myocardial infarction pathophysiology. While normal cardiomyocytes typically do not express TNF-α, it becomes abundant in myocardial tissue following MI due to the activation of cardiomyocytes and local mononuclear macrophages in areas affected by ischemia and anoxia [181]. The systemic inflammatory reaction following AMI is initiated and regulated by the sequential emergence of IL-1β and IL-6 [182]. Moreover, iNOS is upregulated in response to inflammatory triggers. Elevated iNOS expression has been noted in instances of myocardial failure in rats with MI [183]. In the pathophysiology of MI, TGF-β signaling plays a crucial role by mediating both Smad-dependent and non-Smad pathways. This regulation impacts key processes, including fibrosis, leukocyte recruitment, and extracellular matrix (ECM) production through Smad3 activation [184]. In our study, the administration of isoprenaline increased the expression of proinflammatory genes such as IL-1, TGF-β, IL-6, and TNF-α along with iNOS in heart tissues. However, treatment with *R. serpentina* root extract down-regulated this expression. Considering these findings, it is plausible that the decline in the release of inflammatory mediators by *R. serpentina* is linked to the inhibition of NF-κB signaling, ultimately offering significant cardiac protection in isoprenaline-induced rats.

In our research, we conducted a series of morphological tests using various stains to delve further into the development of heart failure following ISO injection. Our findings revealed that high doses of isoprenaline primarily resulted in significant cardiomyocyte necrosis and the accumulation of extracellular matrix collagen. These observations are comparable with a prior study that displayed a marked increase in collagen accumulation in the heart's left ventricle following high levels of catecholamines [185,186]. Furthermore, in ISO-treated rats, the accumulation of collagen fibers was accompanied by a notable presence of mononuclear cells. Following myocardial infarction, oxidative stress mediated by lipid peroxidation and cardiomyocyte necrosis may trigger the migration of monocytes to the injured tissue site [187–189]. Notably, rats given ISO and *R. serpentina* supplementation showed reduced inflammatory cell infiltration and collagen accumulation in the heart. The protective effect is likely due to the antioxidants in *R. serpentina* root extract, which help mitigate cardiomyocyte loss and tissue inflammation.

The kidneys of the control group showed regular glomeruli and tubules. However, rats administered with isoprenaline displayed altered parenchymal cells, glomerular congestion, and tubular hypertrophy. Treatment with the root extract of *R. serpentina* mitigated these structural abnormalities in the rats. Sirius red staining confirmed normal kidney anatomy in the control group, whereas rats administered with isoprenaline exhibited accelerated fibrosis and collagen deposition in kidney sections. Notably, the root extract of *R. serpentina* reduced fibrosis along with collagen accumulation in the kidneys of rats fed isoprenaline.

When it comes to understanding the multi-target, multi-pathway therapeutic processes of complex natural products in the treatment of diseases, network pharmacology is a unique systems biology paradigm that merges computational prediction with experimental confirmation [79–81]. In addition to six important polyphenols derived from *R. serpentina* that show potential as therapies for cardiac hypertrophy, this study identified 141 common targets between proteins linked to disease and molecular targets unique to compounds. It is critical to comprehend these multi-target therapeutic networks in order to advance the creation of evidence-based pharmaceuticals and to construct plausible frameworks for the identification of cardiovascular therapeutics derived from natural product sources [82].

The current gold standard in network pharmacology research is to use multiple computational databases for target prediction to reduce bias in single-database approaches and ensure adequate coverage [80,81]. The identification of cardiac hypertrophy targets employed GeneCards and OMIM databases, resulting in 175 unique disease-associated targets [58,83–86], and for the target prediction major 6 polyphenols of *R. serpentina* found in our study, we have used several databases BATMAN-TCM [49], SuperPred by Charité [50], TargetNet [53], Way2Drug [54], and sea search [56]. Identifying three distinct target groups using Venn diagram analysis is crucial for understanding how *R. serpentina* polyphenols treat cardiac hypertrophy. There were 141 shared targets, or 2.9% of all targets, at the key therapeutic intersection; these represent molecular pathways where polyphenols interact directly with mechanisms linked to cardiac hypertrophy[90,91]. Notably, 4619 molecular targets were identified as polyphenol-specific, accounting for 96.3% of the total targets [73,92]. This underscores the substantial molecular interaction potential of the polyphenolic chemicals found in *R. serpentina.*

The experimental evidence from recent studies that support the cardioprotective effects of *R. serpentina* compounds is consistent with network pharmacology predictions [27,67,77,93–95,97–99]. A number of molecular targets, including PARP-1, VEGFR-2, and aldose reductase, have been identified as having more therapeutic promise for *R. serpentina* in more recent studies [100,190]. Based on functional annotation of target proteins, *R. serpentina* polyphenols have therapeutic potential across various pathways, including PI3K/AKT signaling, MAPK pathways, inflammatory cascades, and apoptosis regulation [97,98,102]. This finding is in line with the pathophysiology of cardiac hypertrophy [97,98,102].

According to the findings of the research conducted on the protein network of *R. serpentina* [103], there are numerous critical hub proteins that have high centrality measures across a variety of characteristics [108–111]. The relative relevance of individual nodes in complex networks can be quantified using these metrics, which are based on the structural placements of the nodes and the connectivity patterns between them [108–111]. Betweenness centrality evaluates a node's position on the shortest pathways connecting other nodes in a network, representing its role as a bridge or intermediate [112]. The closeness centrality of a node is a measure of how well it communicates with the rest of the network based on how close it is to every other node [109]. By utilizing centrality measures on the *R. serpentina* protein network, novel cardiovascular drugs can be more easily discovered [108–111]. This is achieved through a multi-target, synergistic approach that coordinates the modulation of important molecular targets, emulating the pharmacology of traditional medicinal plants [113–116].

Polyphenols from *R. serpentina* exhibit therapeutic mechanisms associated with cardiac hypertrophy [27]. The effects of these polyphenols on cardiac hypertrophy were examined using Metascape, a web-based database integration platform [76]. Twenty terms ($-\log_{10} P \approx 30–50$), with the most notable being pathways in cancer

(hsa05200), gastrin signaling (WP4659), and cellular response to hormone stimulus (GO:0032870), were found to be strongly associated with the relationship between *R. serpentina* polyphenols and cardiac hypertrophy out of 141 common protein targets [76]. Consistent with polyphenolic compounds' known cardioprotective and anti-inflammatory effects, the study noted that cancer-related pathways were the most abundantly represented group (Figures 3 and 4). The notable enhancement of hormone response pathways supports the established use of *R. serpentina* in the treatment of cardiovascular conditions, where hormonal signaling plays a crucial role in cardiac remodeling processes[128,129].

R. serpentina polyphenols target the PI3K/AKT pathway, an important regulator of cardiomyocyte survival, growth, metabolism, and hypertrophic responses. ShinyGO facilitated the mapping of 141 common protein targets among six *R. serpentina* polyphenols and cardiac hypertrophy [71,131,132]. The findings provide a framework for experimental targeting, biomarker identification, and the development of translational strategies for natural product cardiovascular therapeutics, grounded in evidence. The pathway's essential function in cardiac hypertrophy and the prevention of heart failure is underscored by the identification of PI3K/AKT nodes affected by *R. serpentina* polyphenols.

5. Conclusions

The study provided experimental evidence that *R. serpentina* has the potential to improve cardiac and renal function and reduce oxidative stress and apoptosis. The findings suggest that *R. serpentina*, with its high levels of polyphenolic compounds, may protect heart and kidney tissues by enhancing the antioxidant defense system through the Nrf-2-HO-1 pathway, reducing pro-inflammatory cytokine expression, and limiting inflammatory cell infiltration in the myocardium. Based on these *results,* further clinical trials of *R. serpentina* for cardio-renal protection are warranted to translate these preclinical observations into clinical practice.

Supplementary Materials: The following supporting information can be downloaded at: https://media.sciltp.com/articles/others/2603051021013084/JMNP-25120217-supplement-Materials.zip, File S1: The Protein-Protein Interaction Network (PPI) for *R. serpentina*. Results from the protein–protein interaction (PPI) network analysis, including key topological metrics for each node: degree, betweenness centrality, and closeness centrality. File S2: Referenced genes and compound list. This list represents the 141 overlapping targets between cardiac hypertrophy and *R. serpentina* compounds. These were obtained by cross-referencing against 4,760 predicted molecular targets of six polyphenolic constituents of *R. serpentina*, as identified across five in silico platforms: BATMAN-TCM, SuperPred (Charité), TargetNet, Way2Drug, and SEA Search. File S3: Referenced genes and diseases list. This dataset comprises the 141 unique molecular targets associated with cardiac hypertrophy that intersect with those of six *R. serpentina* polyphenols predicted molecular targets. These targets were identified by applying a Venn analysis to data retrieved from the GeneCards and OMIM databases. Prior to filtering, 175 distinct targets had been collated and consolidated from those databases. File S4: Reference compound in *R. Serpentina*. The six polyphenolic compounds of *R. serpentina* were incorporated into the network pharmacology analysis.

Author Contributions: N.S., F.K. and M.A.A. generated the concept and design of this study. M.A.A., F.K., M.B.U., and N.S. also trained K.N.E., M.A., A.U.H.S., P.S., S.S., M.S.A. and M.J.R. on all the research-related activities and supervised and coordinated the whole study. K.N.E., P.S., M.A. and A.U.H.S. carried out animal handling, animal experimentation, and animal sacrifice. K.N.E., M.A., S.S., M.S.A. and A.U.H.S. also performed biochemical analysis. M.A., M.J.R., S.S., N.S. and M.A.A. performed histological analyses. M.A., M.J.R., M.B.U. and F.K. performed the gene expression analyses. K.S.A. and H.H. performed HPLC analysis. K.S.A., H.H., M.B.U., M.J.R. and M.A.A. performed the network pharmacology analysis. M.A.A., N.S., M.S.A., M.B.U. and F.K. performed statistical analysis and interpretation of the results. The draft manuscript was prepared by N.S., M.A.A., M.J.R., M.B.U., H.H. and F.K. All authors have read and agreed to the published version of the manuscript.

Funding: This research received no external funding.

Institutional Review Board Statement: The study was conducted according to the guidelines of the Declaration of Helsinki, and approved by the Institutional Animal Care and Use Committee (IACUC) of the North South University, Bangladesh (IACUC ID-2024/OR-NSU/IACUC/1201).

Informed Consent Statement: Not applicable.

Data Availability Statement: All experimental data for this study are stored in the hard disk drive of the laboratory computer, which will be available upon request.

Acknowledgments: The authors sincerely acknowledge all the logistic support provided by the Department of Pharmaceutical Sciences, North South University, Bangladesh, where this study was conducted.

Conflicts of Interest: The authors declare no conflict of interest. Given the role as Editorial Board Member, Md. Ashraful Alam had no involvement in the peer review of this paper and had no access to information regarding its peer-review process. Full responsibility for the editorial process of this paper was delegated to another editor of the journal.

Use of AI and AI-Assisted Technologies: During the preparation of this work, the authors used the mentioned target prediction tools (PubChem, BATMAN-TCM, SuperPred by Charité, TargetNet, Way2Dru, Similarity Ensemble Approach (SEA), OMIM, GeneCards, UniProt, Venny 2.1, Cytoscape (version 3.10.3), STRING, Metascape, DisGeNET, KEGG API and QuillBot) to

predict molecular targets and interactions for network pharmacology analysis, and results from several databases, and used Grammarly and QuillBot to paraphrase and refine text. After using these tools/services, the authors reviewed and edited the content as needed and take full responsibility for the content of the published article.

References

1. Szlagor, M.; Dybiec, J.; Młynarska, E.; et al. Chronic kidney disease as a comorbidity in heart failure. *Int. J. Mol. Sci.* **2023**, *24*, 2988.
2. Liu, M.; Li, X.-C.; Lu, L.; et al. Cardiovascular disease and its relationship with chronic kidney disease. *Eur. Rev. Med. Pharmacol. Sci.* **2014**, *18*, 2918–2926.
3. Schefold, J.C.; Filippatos, G.; Hasenfuss, G.; et al. Heart failure and kidney dysfunction: Epidemiology, mechanisms and management. *Nat. Rev. Nephrol.* **2016**, *12*, 610–623.
4. Lim, S.H.; Lee, J. Xyloglucan intake attenuates myocardial injury by inhibiting apoptosis and improving energy metabolism in a rat model of myocardial infarction. *Nutr. Res.* **2017**, *45*, 19–29.
5. Hong, K.N.; Fuster, V.; Rosenson, R.S.; et al. How low to go with glucose, cholesterol, and blood pressure in primary prevention of CVD. *J. Am. Coll. Cardiol.* **2017**, *70*, 2171–2185.
6. Hurtubise, J.; McLellan, K.; Durr, K.; et al. The different facets of dyslipidemia and hypertension in atherosclerosis. *Curr. Atheroscler. Rep.* **2016**, *18*, 82.
7. Di Domenico, F.; Tramutola, A.; Butterfield, D.A. Role of 4-hydroxy-2-nonenal (HNE) in the pathogenesis of alzheimer disease and other selected age-related neurodegenerative disorders. *Free Radic. Biol. Med.* **2017**, *111*, 253–261.
8. Zhang, Y.; Martin, S. Redox proteins and radiotherapy. *Clin. Oncol.* **2014**, *26*, 289–300.
9. Zhou, S.; Sun, W.; Zhang, Z.; et al. The role of Nrf2-mediated pathway in cardiac remodeling and heart failure. *Oxidative Med. Cell. Longev.* **2014**, *2014*, 260429.
10. Wang, C.; Pei, Y.-Y.; Ma, Y.-H.; et al. Risk factors for acute kidney injury in patients with acute myocardial infarction. *Chin. Med. J.* **2019**, *132*, 1660–1665.
11. Chiuariu, T.; Șalaru, D.; Ureche, C.; et al. Cardiac and Renal Fibrosis, the Silent Killer in the Cardiovascular Continuum: An Up-to-Date. *J. Cardiovasc. Dev. Dis.* **2024**, *11*, 62.
12. Araujo, M.; Wilcox, C.S. Oxidative stress in hypertension: Role of the kidney. *Antioxid. Redox Signal.* **2014**, *20*, 74–101.
13. AlQudah, M.; Hale, T.M.; Czubryt, M.P. Targeting the renin-angiotensin-aldosterone system in fibrosis. *Matrix Biol.* **2020**, *91*, 92–108.
14. Singh, P.K.; Gari, M.; Choudhury, S.; et al. Oleic acid prevents isoprenaline-induced cardiac injury: Effects on cellular oxidative stress, inflammation and histopathological alterations. *Cardiovasc. Toxicol.* **2020**, *20*, 28–48.
15. Huang, H.; Geng, Q.; Yao, H.; et al. Protective effect of scutellarin on myocardial infarction induced by isoprenaline in rats. *Iran. J. Basic. Med. Sci.* **2018**, *21*, 267.
16. Manolis, A.S.; Manolis, A.A.; Manolis, T.A.; et al. Mitochondrial dysfunction in cardiovascular disease: Current status of translational research/clinical and therapeutic implications. *Med. Res. Rev.* **2021**, *41*, 275–313.
17. Mukherjee, E.; Gantait, S.; Kundu, S.; et al. Biotechnological interventions on the genus Rauvolfia: Recent trends and imminent prospects. *Appl. Microbiol. Biotechnol.* **2019**, *103*, 7325–7354.
18. Anavkar, A.; Patel, N.; Ali, A.; et al. *Plantago ovata* (Isabgol) and *Rauvolfia serpentina* (Indian Snakeroot). In *Herbs, Shrubs, and Trees of Potential Medicinal Benefits*; CRC Press: Boca Raton, FL, USA, 2022; pp. 235–260.
19. Sen, S.; Chakraborty, R. Toward the integration and advancement of herbal medicine: A focus on traditional Indian medicine. *Bot. Targets Ther.* **2015**, *5*, 33–44.
20. Wu, F.; Kerčmar, P.; Zhang, C.; et al. Sarpagan-Ajmalan-Type Indoles: Biosynthesis, structural biology, and chemo-enzymatic significance. *Alkaloids Chem. Biol.* **2016**, *76*, 1–61.
21. Perk, A.A.; Shatynska-Mytsyk, I.; Gerçek, Y.C.; et al. Rutin mediated targeting of signaling machinery in cancer cells. *Cancer Cell Int.* **2014**, *14*, 124.
22. Ciumărnean, L.; Milaciu, M.V.; Runcan, O.; et al. The effects of flavonoids in cardiovascular diseases. *Molecules* **2020**, *25*, 4320.
23. Sánchez, M.; Romero, M.; Gómez-Guzmán, M.; et al. Cardiovascular effects of flavonoids. *Curr. Med. Chem.* **2019**, *26*, 6991–7034.
24. Chaudhary, R.; Singh, B.; Chhillar, A. Ethnomedicinal Importance of *Rauvolfia serpentina* L. Benth. Ex Kurz in the Prevention and Treatment of Diseases. *Nat. Prod. Res. Rev.* **2016**, *3*, 305–326.
25. Alshahrani, M.Y.; Rafi, Z.; Alabdallah, N.M.; et al. A comparative antibacterial, antioxidant, and antineoplastic potential of *Rauwolfia serpentina* (L.) leaf extract with its biologically synthesized gold nanoparticles (R-AuNPs). *Plants* **2021**, *10*, 2278.
26. Gupta, A.K.; Irchhaiya, R.; Misra, C. Free radical scavenging activity of Rauwolfia serpentina rhizome against CCl4 induced liver injury. *Int. J. Pharm.* **2015**, *2*, 123–126.

27. Shah, S.M.A.; Naqvi, S.A.R.; Munir, N.; et al. Antihypertensive and antihyperlipidemic activity of aqueous methanolic extract of Rauwolfia serpentina in albino rats. *Dose-Response* **2020**, *18*, 1559325820942077.
28. Azmi, M.B.; Qureshi, S.A. Rauwolfia serpentina improves altered glucose and lipid homeostasis in fructose-induced type 2 diabetic mice. *Pak. J. Pharm. Sci.* **2016**, *29*, 1619–1624.
29. Rohela, G.K.; Bylla, P.; Korra, R.; et al. Phytochemical screening and antimicrobial activity of leaf, stem, root and their callus extracts in *Rauwolfia tetraphylla*. *Int. J. Agric. Biol.* **2016**, *18*, 521–528.
30. Hossain, H.; Rahman, S.E.; Akbar, P.N.; et al. HPLC profiling, antioxidant and in vivo anti-inflammatory activity of the ethanol extract of *Syzygium jambos* available in Bangladesh. *BMC Res. Notes* **2016**, *9*, 191.
31. Mamun, F.; Rahman, M.M.; Zamila, M.; et al. Polyphenolic compounds of litchi leaf augment kidney and heart functions in 2K1C rats. *J. Funct. Foods* **2020**, *64*, 103662.
32. Clark, J.D.; Gebhart, G.F.; Gonder, J.C.; et al. The 1996 guide for the care and use of laboratory animals. *ILAR J.* **1997**, *38*, 41–48.
33. Lasker, S.; Rahman, M.M.; Parvez, F.; et al. High-fat diet-induced metabolic syndrome and oxidative stress in obese rats are ameliorated by yogurt supplementation. *Sci. Rep.* **2019**, *9*, 20026.
34. Rahman, M.M.; Alimullah, M.; Yasmin, T.; et al. Cardioprotective action of apocynin in isoproterenol-induced cardiac damage is mediated through Nrf-2/HO-1 signaling pathway. *Food Sci. Nutr.* **2024**, *12*, 9108–9122. https://doi.org/10.1002/fsn3.4465.
35. Jahan, I.; Hassan, S.M.H.; Alimullah, M.; et al. Evaluation of fenugreek (*Trigonella foenum-graecum* L.) powder supplementation on metabolic syndrome, oxidative stress and inflammation in high fat diet fed rats. *Pharmacol. Res. Nat. Prod.* **2024**, *5*, 100116. https://doi.org/10.1016/j.prenap.2024.100116.
36. Tracey, W.R.; Tse, J.; Carter, G. Lipopolysaccharide-induced changes in plasma nitrite and nitrate concentrations in rats and mice: Pharmacological evaluation of nitric oxide synthase inhibitors. *J. Pharmacol. Exp. Ther.* **1995**, *272*, 1011–1015.
37. Zahan, T.; Alimullah, M.; Jahan, I.; et al. Baccaurea ramiflora fruit peel powder supplementation prevented inflammatory cell infiltration, oxidative stress, and fibrosis in carbon tetrachloride (CCl4) administered ovariectomized rats. *Phytomed Plus* **2025**, *5*, 100719. https://doi.org/10.1016/j.phyplu.2024.100719.
38. Witko-Sarsat, V.; Friedlander, M.; Capeillère-Blandin, C.; et al. Advanced oxidation protein products as a novel marker of oxidative stress in uremia. *Kidney Int.* **1996**, *49*, 1304–1313.
39. Jahan, I.; Shuvo, A.U.H.; Alimullah, M.; et al. Purple potato extract modulates fat metabolizing genes expression, prevents oxidative stress, hepatic steatosis, and attenuates high-fat diet-induced obesity in male rats. *PLoS ONE* **2025**, *20*, e0318162. https://doi.org/10.1371/journal.pone.0318162.
40. Khan, S.; Rahman, M.M.; Kabir, F.; et al. Trichosanthes dioica Roxb. prevents hepatic inflammation and fibrosis in CCl4-induced ovariectomized rats. *Clin. Nutr. Exp.* **2020**, *33*, 1–17.
41. Alimullah, M.; Rahman, N.; Sornaker, P.; et al. Evaluation of Terminalia arjuna Bark Powder Supplementation on Isoprenaline-Induced Oxidative Stress and Inflammation in the Heart of Long Evans Rats, Understanding the Molecular Mechanism of This Old Medicinal Plant. *J. Med. Nat. Prod.* **2024**, *1*, 100004.
42. Alimullah, M.; Shuvo, A.U.H.; Jahan, I.; et al. Evaluation of the modulating effect of epidermal growth factor receptor inhibitor cetuximab in carbon-tetrachloride induce hepatic fibrosis in rats. *Biochem. Biophys. Rep.* **2024**, *38*, 101689. https://doi.org/10.1016/j.bbrep.2024.101689.
43. Bradley, P.P.; Christensen, R.D.; Rothstein, G. Cellular and extracellular myeloperoxidase in pyogenic inflammation. *Blood* **1982**, *60*, 618–622.
44. Shuvo, A.U.H.; Alimullah, M.; Jahan, I.; et al. Evaluation of Xanthine Oxidase Inhibitors Febuxostat and Allopurinol on Kidney Dysfunction and Histological Damage in Two-Kidney, One-Clip (2K1C) Rats. *Scientifica* **2025**, *2025*, 7932075. https://doi.org/10.1155/sci5/7932075.
45. Jollow, D.; Mitchell, J.; Zampaglione, N.a.; et al. Bromobenzene-induced liver necrosis. Protective role of glutathione and evidence for 3, 4-bromobenzene oxide as the hepatotoxic metabolite. *Pharmacology* **1974**, *11*, 151–169.
46. Kim, S.; Chen, J.; Cheng, T.; et al. PubChem 2023 update. *Nucleic Acids Res.* **2023**, *51*, D1373–D1380.
47. Kim, S.; Thiessen, P.A.; Bolton, E.E.; et al. PubChem substance and compound databases. *Nucleic Acids Res.* **2016**, *44*, D1202–D1213.
48. Kong, X.; Liu, C.; Zhang, Z.; et al. BATMAN-TCM 2.0: An enhanced integrative database for known and predicted interactions between traditional Chinese medicine ingredients and target proteins. *Nucleic Acids Res.* **2024**, *52*, D1110–D1120.
49. Liu, Z.; Guo, F.; Wang, Y.; et al. BATMAN-TCM: A bioinformatics analysis tool for molecular mechANism of traditional Chinese medicine. *Sci. Rep.* **2016**, *6*, 21146.
50. Gallo, K.; Goede, A.; Preissner, R.; et al. SuperPred 3.0: Drug classification and target prediction—A machine learning approach. *Nucleic Acids Res.* **2022**, *50*, W726–W731.
51. Nickel, J.; Gohlke, B.-O.; Erehman, J.; et al. SuperPred: Update on drug classification and target prediction. *Nucleic Acids Res.* **2014**, *42*, W26–W31.

52. Min, S.; Lee, B.; Yoon, S. TargetNet: Functional microRNA target prediction with deep neural networks. *Bioinformatics* **2022**, *38*, 671–677.
53. Yao, Z.-J.; Dong, J.; Che, Y.-J.; et al. TargetNet: A web service for predicting potential drug–target interaction profiling via multi-target SAR models. *J. Comput.-Aided Mol. Des.* **2016**, *30*, 413–424.
54. Druzhilovskiy, D.; Filimonov, D.; Rudik, A.; et al. Way2Drug Platform: From Biological Activity Prediction to Systems Pharmacology. In Proceedings of the 5th Belgrade Bioinformatics Conference, Serbia, Belgrade, 17–20 June 2024; p. 8.
55. Druzhilovskiy, D.; Rudik, A.; Filimonov, D.; et al. Computational platform Way2Drug: From the prediction of biological activity to drug repurposing. *Russ. Chem. Bull.* **2017**, *66*, 1832–1841.
56. Wang, Z.; Liang, L.; Yin, Z.; et al. Improving chemical similarity ensemble approach in target prediction. *J. Cheminform.* **2016**, *8*, 20.
57. Gu, S.; Lai, L. Associating 197 Chinese herbal medicine with drug targets and diseases using the similarity ensemble approach. *Acta Pharmacol. Sin.* **2020**, *41*, 432–438.
58. Amberger, J.S.; Bocchini, C.A.; Schiettecatte, F.; et al. OMIM. org: Online Mendelian Inheritance in Man (OMIM®), an online catalog of human genes and genetic disorders. *Nucleic Acids Res.* **2015**, *43*, D789–D798.
59. Hamosh, A.; Scott, A.F.; Amberger, J.S.; et al. Online Mendelian Inheritance in Man (OMIM), a knowledgebase of human genes and genetic disorders. *Nucleic Acids Res.* **2005**, *33*, D514–D517.
60. Amberger, J.S.; Bocchini, C.A.; Scott, A.F.; et al. OMIM. org: Leveraging knowledge across phenotype–gene relationships. *Nucleic Acids Res.* **2019**, *47*, D1038–D1043.
61. Safran, M.; Rosen, N.; Twik, M.; et al. The genecards suite. In *Practical Guide to Life Science Databases*; Springer Nature: Singapore, 2021; pp. 27–56.
62. Stelzer, G.; Rosen, N.; Plaschkes, I.; et al. The GeneCards suite: From gene data mining to disease genome sequence analyses. *Curr. Protoc. Bioinform.* **2016**, *54*, 1–30.
63. Consortium, U. UniProt: A worldwide hub of protein knowledge. *Nucleic Acids Res.* **2019**, *47*, D506–D515.
64. The UniProt Consortium. UniProt: The universal protein knowledgebase in 2021. *Nucleic Acids Res.* **2021**, *49*, D480–D489.
65. Wang, Z.; Li, X.; Chen, H.; et al. Decreased HLF expression predicts poor survival in lung adenocarcinoma. *Med. Sci. Monit. Int. Med. J. Exp. Clin. Res.* **2021**, *27*, e929333-1.
66. Zúñiga-Hernández, S.R.; García-Iglesias, T.; Macías-Carballo, M.; et al. A Bioinformatic Assay of Quercetin in Gastric Cancer. *Int. J. Mol. Sci.* **2024**, *25*, 7934.
67. Shannon, P.; Markiel, A.; Ozier, O.; et al. Cytoscape: A software environment for integrated models of biomolecular interaction networks. *Genome Res.* **2003**, *13*, 2498–2504.
68. Liu, H.; Yang, S.; Chen, B.; et al. Integrating network pharmacology and molecular docking to explore the pharmacological mechanism of tanshinone IIA in improving chronic obstructive pulmonary disease. *Medicine* **2025**, *104*, e41638.
69. Szklarczyk, D.; Nastou, K.; Koutrouli, M.; et al. The STRING database in 2025: Protein networks with directionality of regulation. *Nucleic Acids Res.* **2025**, *53*, D730–D737.
70. Wahyuni, S.; Jamil, A.S.; Muchlisin, M.A. A Network Pharmacology of *Camellia sinensis* (Green Tea*). Proc. Int. Pharm. Ulul Albab Conf. Semin.* **2023**, 216–224. https://doi.org/10.18860/planar.v3i0.2487.
71. Ge, S.X.; Jung, D.; Yao, R. ShinyGO: A graphical gene-set enrichment tool for animals and plants. *Bioinformatics* **2020**, *36*, 2628–2629.
72. Bisht, A.; Tewari, D.; Kumar, S.; et al. Network pharmacology-based approach to investigate the molecular targets and molecular mechanisms of Rosmarinus officinalis L. for treating aging-related disorders. *Biogerontology* **2024**, *25*, 793–808.
73. Hedayati, N.; Yaghoobi, A.; Salami, M.; et al. Impact of polyphenols on heart failure and cardiac hypertrophy: Clinical effects and molecular mechanisms. *Front. Cardiovasc. Med.* **2023**, *10*, 1174816.
74. Sun, G.; Qiu, Z.; Wang, W.; et al. Flavonoids extraction from propolis attenuates pathological cardiac hypertrophy through PI3K/AKT signaling pathway. *Evid. Based Complement. Altern. Med.* **2016**, *2016*, 6281376.
75. Guan, P.; Sun, Z.-M.; Wang, N.; et al. Resveratrol prevents chronic intermittent hypoxia-induced cardiac hypertrophy by targeting the PI3K/AKT/mTOR pathway. *Life Sci.* **2019**, *233*, 116748.
76. Zhou, Y.; Zhou, B.; Pache, L.; et al. Metascape provides a biologist-oriented resource for the analysis of systems-level datasets. *Nat. Commun.* **2019**, *10*, 1523.
77. Ren, S.; Shen, L.; Lin, S.; et al. Mechanistic analysis of resveratrol in cardiac hypertrophy by network pharmacology and animal experiments. *Mol. Med. Rep.* **2022**, *26*, 324.
78. Wang, X.; Wang, Y.; Yuan, T.; et al. Network pharmacology provides new insights into the mechanism of traditional Chinese medicine and natural products used to treat pulmonary hypertension. *Phytomedicine* **2024**, *135*, 156062.
79. Yu, W.; Weng, Y.; Wang, J.; et al. Network Pharmacology Approach and Partial Experimental Validation of Aidi Injection Solution for the Treatment of Colorectal Cancer. *Nat. Prod. Commun.* **2024**, *19*, 1934578X241239169.
80. Peng, Y.; Zhu, G.; Ma, Y.; et al. Network Pharmacology–Based Prediction and Pharmacological Validation of Effects of Astragali Radix on Acetaminophen-Induced Liver Injury. *Front. Med.* **2022**, *9*, 697644.

81. Yang, X.; Qin, Y.; Zhou, H. Deciphering the Pharmacological Mechanisms of Wen-Jing-Zhi-Tong Decoction in Treating Primary Dysmenorrhea by UPLC-Q-Exactive-Orbitrap-MS/MS with GC-MS and Network Pharmacology. *Comb. Chem. High. Throughput Screen.* **2025**, *28*, 1011–1025.
82. Liu, M.; Zheng, L.; Zhang, Y.; et al. Mechanistic insights into pachymic acid's action on triple-negative breast Cancer through TOP2A targeting. *Sci. Rep.* **2025**, *15*, 2856.
83. Jiang, S.; Huang, C.; Wang, S.; et al. Network pharmacology-based strategy for predicting therapy targets of Citri Reticulatae Pericarpium on myocardial hypertrophy. *BioMed Res. Int.* **2022**, *2022*, 4293265.
84. Wang, J.; Yang, Z.; Jiang, J.; et al. Systematically Investigating the Pharmacological Mechanism of Momordica grosvenori in the Treatment of Spinal Cord Injury by Network Pharmacology and Experimental Verification. *Evid. Based Complement. Altern. Med.* **2023**, *2023*, 1638966.
85. Zhang, Z.; Wang, C. Exploring key genes and pathways of cardiac hypertrophy based on bioinformatics. *Dis. Markers* **2022**, *2022*, 2081590.
86. Safran, M.; Dalah, I.; Alexander, J.; et al. GeneCards Version 3: The human gene integrator. *Database* **2010**, *2010*, baq020.
87. Huang, X.; Huang, F.; Shu, H.; et al. Garlic's anti-mastitis mechanism studied via network pharmacology & molecular docking. In Proceedings of the 2025 5th International Conference on Bioinformatics and Intelligent Computing, Shenyang, China, 10–12 January 2025; pp. 385–390.
88. Kong, J.; Huang, X.; Yang, X.; et al. Network pharmacology-based prediction of potential targets of ethnic medicine *Blumea balsamifera* (L.) DC acting on anti-infammatory effect. *J. Phys. Conf. Ser.* **2020**, *1486*, 022032.
89. Shi, X.; Luo, Y.; Yang, L.; et al. Protective effect of Gastrodia elata Blume in a Caenorhabditis elegans model of Alzheimer's disease based on network pharmacology. *Biomed. Rep.* **2023**, *18*, 37.
90. Gong, K.; Yang, K.; Xie, T.; et al. Identification of circRNA-miRNA-mRNA regulatory network and its role in cardiac hypertrophy. *PLoS ONE* **2023**, *18*, e0279638.
91. Chen, L.; Li, M.; Shen, M.; et al. Bioinformatics exploration of potential common therapeutic targets for systemic and pulmonary arterial hypertension-induced myocardial hypertrophy: Common therapeutic target for left and right ventricular hypertrophy. *Acta Biochim. Biophys. Sin.* **2023**, *55*, 831.
92. Singh, M. Evaluating the therapeutic efficiency and drug targeting ability of alkaloids present in *Rauwolfia serpentina*. *Int. J. Green Pharm.* **2017**, *11*, 132–142.
93. Ma, Y.-Q.; Zhang, M.; Sun, Z.-H.; et al. Identification of anti-gastric cancer effects and molecular mechanisms of resveratrol: From network pharmacology and bioinformatics to experimental validation. *World J. Gastrointest. Oncol.* **2024**, *16*, 493.
94. Wijaya, P.; Tallei, T.E.; Tendean, L.E.N.; et al. Network Pharmacology Insights into Broccoli Microgreens for Prostate Cancer. *Heca J. Appl. Sci.* **2025**, *3*, 1–16.
95. Li, S.; Fan, T.-P.; Jia, W.; et al. Network pharmacology in traditional Chinese medicine. *Evid. -Based Complement. Altern. Med. Ecam* **2014**, *2014*, 138460.
96. Chang, C.; Jia, R.; Fang, B.; et al. Network pharmacological analysis and in vitro testing of the rutin effects on triple-negative breast cancer. *Open Med.* **2025**, *20*, 20241079.
97. Liu, Y.; Li, Q.; Shao, C.; et al. Exploring the potential mechanisms of guanxinshutong capsules in treating pathological cardiac hypertrophy based on network pharmacology, computer-aided drug design, and animal experiments. *ACS Omega* **2024**, *9*, 18083–18098.
98. Wu, Q.; Zhou, Q.; Wan, C.; et al. Mechanism Actions of Coniferyl Alcohol in Improving Cardiac Dysfunction in Renovascular Hypertension Studied by Experimental Verification and Network Pharmacology. *Int. J. Mol. Sci.* **2024**, *25*, 10063.
99. Zhou, L.; Ding, H.-m.; Du, Y.; et al. Liquiritin ameliorates acute myocardial infarction via the COX-2/NLRP3 signaling pathway: Network pharmacology and experimental validation. *Ital. J. Food Sci.* **2024**, *36*, 1.
100. Pathania, S.; Randhawa, V.; Bagler, G. Prospecting for novel plant-derived molecules of Rauvolfia serpentina as inhibitors of Aldose Reductase, a potent drug target for diabetes and its complications. *PLoS ONE* **2013**, *8*, e61327.
101. Azmi, M.B.; Sultana, S.; Naeem, S.; et al. In silico investigation on alkaloids of Rauwolfia serpentina as potential inhibitors of 3-hydroxy-3-methyl-glutaryl-CoA reductase. *Saudi J. Biol. Sci.* **2021**, *28*, 731–737.
102. Yang, K.; Shan, X.; Yang, S.; et al. Network pharmacology integrated with experimental validation to elucidate the mechanisms of action of the Guizhi-Gancao Decoction in the treatment of phenylephrine-induced cardiac hypertrophy. *Pharm. Biol.* **2024**, *62*, 456–471.
103. Ramly, B.; Afiqah-Aleng, N.; Mohamed-Hussein, Z.-A. Protein–protein interaction network analysis reveals several diseases highly associated with polycystic ovarian syndrome. *Int. J. Mol. Sci.* **2019**, *20*, 2959.
104. Xia, J.; Benner, M.J.; Hancock, R.E. NetworkAnalyst-integrative approaches for protein–protein interaction network analysis and visual exploration. *Nucleic Acids Res.* **2014**, *42*, W167–W174.

105. Szklarczyk, D.; Gable, A.L.; Lyon, D.; et al. STRING v11: Protein–protein association networks with increased coverage, supporting functional discovery in genome-wide experimental datasets. *Nucleic Acids Res.* **2019**, *47*, D607–D613.
106. Rezaei-Tavirani, M.; Rezaei-Tavirani, S.; Mansouri, V.; et al. Protein-protein interaction network analysis for a biomarker panel related to human esophageal adenocarcinoma. *Asian Pac. J. Cancer Prev.* **2017**, *18*, 3357.
107. Majeed, A.; Mukhtar, S. Protein–protein interaction network exploration using cytoscape. In *Protein-Protein Interactions: Methods and Protocols*; Springer: New York, NY, USA, 2023; pp. 419–427.
108. Kardos, O.; London, A.; Vinkó, T. Stability of network centrality measures: A numerical study. *Soc. Netw. Anal. Min.* **2020**, *10*, 80.
109. Sabah, L.; Şimşek, M. A new fast entropy-based method to generate composite centrality measures in complex networks. *Concurr. Comput. Pract. Exp.* **2023**, *35*, e7657.
110. Mukhtar, M.F.; Anuar, S.H.H.; Abas, Z.A.; et al. Bibliometric Analysis of the Global Trend in Centrality Measures. *Int. J. Acad. Res. Bus. Soc. Sci.* **2024**, *14*, 1078–1098.
111. Xiong, W.; Xie, L.; Zhou, S.; et al. The centrality of cancer proteins in human protein-protein interaction network: A revisit. *Int. J. Comput. Biol. Drug Des.* **2014**, *7*, 146–156.
112. Giles, A.P.; Georgiou, O.; Dettmann, C.P. Betweenness centrality in dense random geometric networks. In Proceedings of the 2015 IEEE International Conference on Communications (ICC), London, UK, 8–12 June 2015; pp. 6450–6455.
113. Ochieng, P.J.; Hussain, A.; Dombi, J.; et al. An efficient weighted network centrality approach for exploring mechanisms of action of the Ruellia herbal formula for treating rheumatoid arthritis. *Appl. Netw. Sci.* **2023**, *8*, 7.
114. Chiranjeevi, M.; Dhuli, V.S.; Enduri, M.K.; et al. Icdc: Ranking influential nodes in complex networks based on isolating and clustering coefficient centrality measures. *IEEE Access* **2023**, *11*, 126195–126208.
115. Nandini, Y.; Lakshmi, T.J.; Enduri, M.K.; et al. Link prediction in complex networks using average centrality-based similarity score. *Entropy* **2024**, *26*, 433.
116. Parisutham, N. The Impact of Centrality Measures in Protein–Protein Interaction Networks: Tools, Databases, Challenges and Future Directions. *J. Comput. Biophys. Chem.* **2024**, *23*, 815–836.
117. Madonna, R.; Geng, Y.-J.; Bolli, R.; et al. Co-activation of nuclear factor-κB and myocardin/serum response factor conveys the hypertrophy signal of high insulin levels in cardiac myoblasts. *J. Biol. Chem.* **2014**, *289*, 19585–19598.
118. Jin, L.; Hou, P. Yixin-Fumai granules modulate autophagy through the PI3K/AKT/FOXO pathway and lead to amelioration of aging mice with sick sinus syndrome. *Immun. Ageing* **2024**, *21*, 46.
119. Zhao, M.; Feng, L.; Li, W. Network Pharmacology and Experimental Verification: SanQi-DanShen Treats Coronary Heart Disease by Inhibiting the PI3K/AKT Signaling Pathway. *Drug Des. Dev. Ther.* **2024**, *18*, 4529–4550.
120. Zhang, Y.; Zhang, X.; Zhang, X.; et al. Molecular targets and pathways contributing to the effects of wenxin keli on atrial fibrillation based on a network pharmacology approach. *Evid. Based Complement. Altern. Med.* **2020**, *2020*, 8396484.
121. Chen, C.; Zou, L.-X.; Lin, Q.-Y.; et al. Resveratrol as a new inhibitor of immunoproteasome prevents PTEN degradation and attenuates cardiac hypertrophy after pressure overload. *Redox Biol.* **2019**, *20*, 390–401.
122. Aoyagi, T.; Matsui, T. Phosphoinositide-3 kinase signaling in cardiac hypertrophy and heart failure. *Curr. Pharm. Des.* **2011**, *17*, 1818–1824.
123. Zhao, A.; Zhang, X.; Hu, G.; et al. Novel Gene Signatures for Prostate Cancer Detection: Network Centralitybased Screening with Experimental Validation. *Curr. Bioinform.* **2023**, *18*, 842–852.
124. Ni, X.; Bao, H.; Guo, J.; et al. Discussion on the mechanism of Danggui Sini decoction in treating diabetic foot based on network pharmacology and molecular docking and verification of the curative effect by meta-analysis. *Front. Endocrinol.* **2024**, *15*, 1347021.
125. Azmi, M.B.; Qureshi, S.A. Methanolic root extract of Rauwolfia serpentina benth improves the glycemic, antiatherogenic, and cardioprotective indices in alloxan-induced diabetic mice. *Adv. Pharmacol. Pharm. Sci.* **2012**, *2012*, 376429.
126. Pathania, S.; Ramakrishnan, S.M.; Randhawa, V.; et al. SerpentinaDB: A database of plant-derived molecules of *Rauvolfia serpentina*. *BMC Complement. Altern. Med.* **2015**, *15*, 262.
127. Afsheen, N.; Jahan, N.; Ijaz, M.; et al. Cardioprotective and metabolomic profiling of selected medicinal plants against oxidative stress. *Oxidative Med. Cell. Longev.* **2018**, *2018*, 9819360.
128. Netala, V.R.; Teertam, S.K.; Li, H.; et al. A comprehensive review of cardiovascular disease management: Cardiac biomarkers, imaging modalities, pharmacotherapy, surgical interventions, and herbal remedies. *Cells* **2024**, *13*, 1471.
129. Ananta, M.F.; Oyshi, S.A.; Mim, M.M.A.; et al. Multipurpose Drug from *Rouwolfia serpentina* and *Nigella sativa*: A Herbal Approach to Treat Hypertension and Hyperlipidemia in Experimental Rodent Model. *J. Complement. Altern. Med. Res.* **2023**, *24*, 9–15.
130. Piñero, J.; Bravo, À.; Queralt-Rosinach, N.; et al. DisGeNET: A comprehensive platform integrating information on human disease-associated genes and variants. *Nucleic Acids Res.* **2017**, *45*, D833–D839. https://doi.org/10.1093/nar/gkw943.
131. Qin, W.; Cao, L.; Massey, I.Y. Role of PI3K/Akt signaling pathway in cardiac fibrosis. *Mol. Cell. Biochem.* **2021**, *476*, 4045–4059.

132. Ghafouri-Fard, S.; Khanbabapour Sasi, A.; Hussen, B.M.; et al. Interplay between PI3K/AKT pathway and heart disorders. *Mol. Biol. Rep.* **2022**, *49*, 9767–9781.
133. McLean, B.A.; Zhabyeyev, P.; Pituskin, E.; et al. PI3K inhibitors as novel cancer therapies: Implications for cardiovascular medicine. *J. Card. Fail.* **2013**, *19*, 268–282.
134. Zhang, P.; Li, H.; Zhang, A.; et al. Mechanism of myocardial fibrosis regulation by IGF-1R in atrial fibrillation through the PI3K/Akt/FoxO3a pathway. *Biochem. Cell Biol.* **2023**, *101*, 432–442.
135. Pandey, P.; Khan, F.; Upadhyay, T.K.; et al. New insights about the PDGF/PDGFR signaling pathway as a promising target to develop cancer therapeutic strategies. *Biomed. Pharmacother.* **2023**, *161*, 114491.
136. Ivey, M.J.; Kuwabara, J.T.; Riggsbee, K.L.; et al. Platelet-derived growth factor receptor-α is essential for cardiac fibroblast survival. *Am. J. Physiol.-Heart Circ. Physiol.* **2019**, *317*, H330–H344.
137. Mouton, A.J. Platelet-Derived Growth Factors: A New Therapeutic Opportunity for Treating Cardiac Fibrosis? *Basic Transl. Sci.* **2023**, *8*, 675–676.
138. Asli, N.S.; Xaymardan, M.; Forte, E.; et al. PDGFRα signaling in cardiac fibroblasts modulates quiescence, metabolism and self-renewal, and promotes anatomical and functional repair. *BioRxiv* **2017**, 225979. https://doi.org/10.1101/225979.
139. McMullen, J.R.; Amirahmadi, F.; Woodcock, E.A.; et al. Protective effects of exercise and phosphoinositide 3-kinase (p110α) signaling in dilated and hypertrophic cardiomyopathy. *Proc. Natl. Acad. Sci.* **2007**, *104*, 612–617.
140. Proud, C.G. Ras, PI3-kinase and mTOR signaling in cardiac hypertrophy. *Cardiovasc. Res.* **2004**, *63*, 403–413.
141. Gao, W.; Guo, N.; Zhao, S.; et al. HTR2A promotes the development of cardiac hypertrophy by activating PI3K-PDK1-AKT-mTOR signaling. *Cell Stress. Chaperones* **2020**, *25*, 899–908.
142. Di, R.; Wu, X.; Chang, Z.; et al. S6K inhibition renders cardiac protection against myocardial infarction through PDK1 phosphorylation of Akt. *Biochem. J.* **2012**, *441*, 199–207.
143. Völkers, M.; Toko, H.; Doroudgar, S.; et al. Pathological hypertrophy amelioration by PRAS40-mediated inhibition of mTORC1. *Proc. Natl. Acad. Sci.* **2013**, *110*, 12661–12666.
144. Sharma, A.K.; Bhatia, S.; Al-Harrasi, A.; et al. Crosstalk between GSK-3β-actuated molecular cascades and myocardial physiology. *Heart Fail. Rev.* **2021**, *26*, 1495–1504.
145. Pillai, V.B.; Sundaresan, N.R.; Gupta, M.P. Regulation of Akt signaling by sirtuins: Its implication in cardiac hypertrophy and aging. *Circ. Res.* **2014**, *114*, 368–378.
146. Selvetella, G.; Hirsch, E.; Notte, A.; et al. Adaptive and maladaptive hypertrophic pathways: Points of convergence and divergence. *Cardiovasc. Res.* **2004**, *63*, 373–380.
147. Bernardo, V.S.; Torres, F.F.; Da Silva, D.G.H. FoxO3 and oxidative stress: A multifaceted role in cellular adaptation. *J. Mol. Med.* **2023**, *101*, 83–99.
148. Xin, Z.; Ma, Z.; Jiang, S.; et al. FOXOs in the impaired heart: New therapeutic targets for cardiac diseases. *Biochim. Et. Biophys. Acta (BBA)-Mol. Basis Dis.* **2017**, *1863*, 486–498.
149. Shafaati, T.; Gopal, K. Forkhead box O1 transcription factor; a therapeutic target for diabetic cardiomyopathy. *J. Pharm. Pharm. Sci.* **2024**, *27*, 13193.
150. Meng, X.; Cui, J.; He, G. Bcl-2 is involved in cardiac hypertrophy through PI3K-Akt pathway. *BioMed Res. Int.* **2021**, *2021*, 6615502.
151. Agrawal, Y.O.; Sharma, P.K.; Shrivastava, B.; et al. Hesperidin produces cardioprotective activity via PPAR-γ pathway in ischemic heart disease model in diabetic rats. *PLoS ONE* **2014**, *9*, e111212.
152. Mohany, M.; Ahmed, M.M.; Al-Rejaie, S.S. Molecular mechanistic pathways targeted by natural antioxidants in the prevention and treatment of chronic kidney disease. *Antioxidants* **2021**, *11*, 15.
153. Vasques-Nóvoa, F.; Angélico-Gonçalves, A.; Alvarenga, J.M.; et al. Myocardial oedema: Pathophysiological basis and implications for the failing heart. *ESC Heart Fail.* **2022**, *9*, 958–976.
154. Losada-Barreiro, S.; Bravo-Diaz, C. Free radicals and polyphenols: The redox chemistry of neurodegenerative diseases. *Eur. J. Med. Chem.* **2017**, *133*, 379–402.
155. Jiang, M.; Xie, X.; Cao, F.; et al. Mitochondrial metabolism in myocardial remodeling and mechanical unloading: Implications for ischemic heart disease. *Front. Cardiovasc. Med.* **2021**, *8*, 789267.
156. Aydin, S.; Ugur, K.; Aydin, S.; et al. Biomarkers in acute myocardial infarction: Current perspectives. *Vasc. Health Risk Manag.* **2019**, *15*, 1–10.
157. Battelli, M.G.; Polito, L.; Bortolotti, M.; et al. Xanthine oxidoreductase-derived reactive species: Physiological and pathological effects. *Oxidative Med. Cell. Longev.* **2016**, *2016*, 3527579.
158. Zhang, S.; Wang, Y.; Cheng, J.; et al. Hyperuricemia and cardiovascular disease. *Curr. Pharm. Des.* **2019**, *25*, 700–709.
159. Sánchez-Lozada, L.G. The pathophysiology of uric acid on renal diseases. In *Uric Acid in Chronic Kidney Disease*; Karger Publishers: Basel, Switzerland, 2018; Volume 192, pp. 17–24.
160. Zhang, W. Uric acid en route to gout. *Adv. Clin. Chem.* **2023**, *116*, 209–275.

161. Damman, K.; Valente, M.A.; Voors, A.A.; et al. Renal impairment, worsening renal function, and outcome in patients with heart failure: An updated meta-analysis. *Eur. Heart J.* **2014**, *35*, 455–469.
162. Chen, X.; Li, X.; Xu, X.; et al. Ferroptosis and cardiovascular disease: Role of free radical-induced lipid peroxidation. *Free Radic. Res.* **2021**, *55*, 405–415.
163. Vida, C.; Oliva, C.; Yuste, C.; et al. Oxidative stress in patients with advanced CKD and renal replacement therapy: The key role of peripheral blood leukocytes. *Antioxidants* **2021**, *10*, 1155.
164. Dal Monte, M.; Fornaciari, I.; Nicchia, G.P.; et al. β3-adrenergic receptor activity modulates melanoma cell proliferation and survival through nitric oxide signaling. *Naunyn-Schmiedeberg's Arch. Pharmacol.* **2014**, *387*, 533–543.
165. Kaptoge, S.; Seshasai, S.R.K.; Gao, P.; et al. Inflammatory cytokines and risk of coronary heart disease: New prospective study and updated meta-analysis. *Eur. Heart J.* **2014**, *35*, 578–589.
166. Seropian, I.M.; Toldo, S.; Van Tassell, B.W.; et al. Anti-inflammatory strategies for ventricular remodeling following ST-segment elevation acute myocardial infarction. *J. Am. Coll. Cardiol.* **2014**, *63*, 1593–1603.
167. Satoh, N.; Nakamura, M.; Suzuki, A.; et al. Effects of nitric oxide on renal proximal tubular Na+ transport. *BioMed Res. Int.* **2017**, *2017*, 6871081.
168. de Brum, G.F.; Bochi, G.V. Are Advanced Oxidation Protein Products (AOPPs) Levels Altered in Neuropsychiatric Disorders? An Integrative Review. *Mol. Neurobiol.* **2024**, 61, 9043–9059.
169. Ou, H.; Huang, Z.; Mo, Z.; et al. The characteristics and roles of advanced oxidation protein products in atherosclerosis. *Cardiovasc. Toxicol.* **2017**, *17*, 1–12.
170. Wan, C.; Su, H.; Zhang, C. Role of NADPH oxidase in metabolic disease-related renal injury: An update. *Oxidative Med. Cell. Longev.* **2016**, *2016*, 7813072.
171. Gryszczyńska, B.; Formanowicz, D.; Budzyń, M.; et al. Advanced oxidation protein products and carbonylated proteins as biomarkers of oxidative stress in selected atherosclerosis-mediated diseases. *BioMed Res. Int.* **2017**, *2017*, 4975264.
172. Lin, W.; Chen, H.; Chen, X.; et al. The roles of neutrophil-derived myeloperoxidase (MPO) in diseases: The new progress. *Antioxidants* **2024**, *13*, 132.
173. Khan, A.A.; Alsahli, M.A.; Rahmani, A.H. Myeloperoxidase as an active disease biomarker: Recent biochemical and pathological perspectives. *Med. Sci.* **2018**, *6*, 33.
174. Ghali, J.R.; Wang, Y.M.; Holdsworth, S.R.; et al. Regulatory T cells in immune-mediated renal disease. *Nephrology* **2016**, *21*, 86–96.
175. Costa, T.J.; Barros, P.R.; Arce, C.; et al. The homeostatic role of hydrogen peroxide, superoxide anion and nitric oxide in the vasculature. *Free Radic. Biol. Med.* **2021**, *162*, 615–635.
176. Nandi, A.; Yan, L.-J.; Jana, C.K.; et al. Role of catalase in oxidative stress-and age-associated degenerative diseases. *Oxidative Med. Cell. Longev.* **2019**, *2019*, 9613090.
177. Otterbein, L.E.; Foresti, R.; Motterlini, R. Heme oxygenase-1 and carbon monoxide in the heart: The balancing act between danger signaling and pro-survival. *Circ. Res.* **2016**, *118*, 1940–1959.
178. Akter, N.; Chowdhury, F.I.; Selim, S.; et al. Polyphenolics in ramontchi protect cardiac tissues via suppressing isoprenaline-induced oxidative stress and inflammatory responses in Long-Evans rats. *J. Funct. Foods* **2020**, *75*, 104250.
179. Saha, S.; Buttari, B.; Panieri, E.; et al. An overview of Nrf2 signaling pathway and its role in inflammation. *Molecules* **2020**, *25*, 5474.
180. Prabhu, S.D.; Frangogiannis, N.G. The biological basis for cardiac repair after myocardial infarction: From inflammation to fibrosis. *Circ. Res.* **2016**, *119*, 91–112.
181. Tian, M.; Yuan, Y.-C.; Li, J.-Y.; et al. Tumor necrosis factor-α and its role as a mediator in myocardial infarction: A brief review. *Chronic Dis. Transl. Med.* **2015**, *1*, 18–26.
182. Shahrivari, M.; Wise, E.; Resende, M.; et al. Peripheral blood cytokine levels after acute myocardial infarction: IL-1β–and IL-6–related impairment of bone marrow function. *Circ. Res.* **2017**, *120*, 1947–1957.
183. Chen, C.; Du, P.; Wang, J. Paeoniflorin ameliorates acute myocardial infarction of rats by inhibiting inflammation and inducible nitric oxide synthase signaling pathways. *Mol. Med. Rep.* **2015**, *12*, 3937–3943.
184. Frangogiannis, N.G. The role of transforming growth factor (TGF)-β in the infarcted myocardium. *J. Thorac. Dis.* **2017**, *9*, S52.
185. Soriano, F.G.; Guido, M.C.; Barbeiro, H.V.; et al. Endotoxemic myocardial dysfunction: Subendocardial collagen deposition related to coronary driving pressure. *Shock* **2014**, *42*, 472–479.
186. Ferreira, V.M.; Marcelino, M.; Piechnik, S.K.; et al. Pheochromocytoma is characterized by catecholamine-mediated myocarditis, focal and diffuse myocardial fibrosis, and myocardial dysfunction. *J. Am. Coll. Cardiol.* **2016**, *67*, 2364–2374.
187. Neri, M.; Fineschi, V.; Di Paolo, M.; et al. Cardiac oxidative stress and inflammatory cytokines response after myocardial infarction. *Curr. Vasc. Pharmacol.* **2015**, *13*, 26–36.
188. Saparov, A.; Ogay, V.; Nurgozhin, T.; et al. Role of the immune system in cardiac tissue damage and repair following myocardial infarction. *Inflamm. Res.* **2017**, *66*, 739–751.

189. Oliveira, J.B.; Soares, A.A.; Sposito, A.C. Inflammatory response during myocardial infarction. *Adv. Clin. Chem.* **2018**, *84*, 39–79.
190. Abuzenadah, A.M.; Al-Sayes, F.; Mahafujul Alam, S.S.; et al. Elucidating antiangiogenic potential of *Rauwolfia serpentina*: VEGFR-2 targeting-based molecular docking study. *Evid. Based Complement. Altern. Med.* **2022**, *2022*, 6224666.